Understanding the Formation and Intensification Process of Several Cyclonic Systems over the Bay of Bengal using the Revised Genesis Potential Parameter Index

Md. Shakil Hossain
Department of Mathematics, Khulna University of Engineering & Technology

Md. Saddam Hossain
Department of Mathematics, Bangladesh University of Engineering and Technology

Most. Fatema Amin Akhi
Department of Mathematics, Dhaka University of Engineering and Technology

Md. Abdus Samad
Department of Applied Mathematics, University of Dhaka

他

https://doi.org/10.5109/7183355

出版情報：Evergreen. 11 (2), pp.736-755, 2024-06. 九州大学グリーンテクノロジー研究教育センター
バージョン：

Understanding the Formation and Intensification Process of Several Cyclonic Systems over the Bay of Bengal using the Revised Genesis Potential Parameter Index

Md. Shakil Hossain[1, *], Md. Saddam Hossain[2], Most. Fatema Amin Akhi[3], Md. Abdus Samad[4], Muhammad Abul Kalam Mallik[5]

[1]Department of Mathematics, Khulna University of Engineering & Technology, Bangladesh

[2]Department of Mathematics, Bangladesh University of Engineering and Technology, Bangladesh

[3]Department of Mathematics, Dhaka University of Engineering and Technology, Bangladesh

[4]Department of Applied Mathematics, University of Dhaka, Bangladesh

[5]Bangladesh Meteorological Department, Bangladesh

*Author to whom correspondence should be addressed:
E-mail: shakil@math.kuet.ac.bd

(Received November 1, 2023; Revised May 29, 2024; Accepted June 2, 2024).

Abstract: The Bay of Bengal experiences numerous low-pressure systems almost throughout the year. However, only a small fraction of these systems intensify into catastrophic storms. Predicting the cyclonic systems' formation and intensification process has long been a crucial but challenging task due to their short lifespan and rapid intensity variations. In this study, an attempt has been made to develop the Revised Genesis Potential Parameter Index (RGPPI) and assess its effectiveness in determining the suitability of the existing environment for cyclone formation. In the present study, numerical simulation has been performed using the advanced Weather Research and Forecasting model (WRF-ARW). The WRF-ARW model has run on a single domain with a 10-kilometer horizontal resolution to simulate the formation and intensification processes of four cyclonic systems of varying intensities over the Bay of Bengal. The results suggest that RGPPI can be useful for predicting cyclonic system development. Using RGPPI, we can forecast changes in cyclonic systems and the corresponding environmental conditions with a lead time of 24 to 48 hours in advance. It is found that non-developing systems typically exhibit a mean RGPPI value equal to or below 30.0, while developing systems may surpass this threshold. Furthermore, it is also observed that systems with higher severity levels could have average RGPPI values ranging from 3 to 8 times greater than the 30.0 threshold value. This study is expected to enhance researchers' current comprehension of tropical cyclone genesis and intensity prediction.

Keywords: Tropical cyclone, genesis, Bay of Bengal, sea surface temperature, RGPPI

1. Introduction

A Tropical Cyclone (TC) refers to a rotating system of low pressure that typically originates over warm tropical oceans or seas. These cyclones are characterized by low pressure, powerful winds, intense rainfall, and resulting floods. Among the most dangerous and damaging weather phenomena, TCs have profound societal and economic impacts on Earth[1, 2]. Historical data indicates an annual formation of about 80-90 TCs across various ocean basins globally [3]. The North Indian Ocean, encompassing the Arabian Sea and the Bay of Bengal (BoB), contributes roughly 7% to this global TC count [4]. The specific oceanic and atmospheric conditions make BoB more conducive to TC formation compared to the Arabian Sea. Approximately three to four TCs form within the BoB each year [5], and these storms rank among the most lethal on a global scale [6]. TCs pose significant problems for the Indian subcontinent, particularly in the coastal region, due to their devastating impacts. These intense TCs accompanied by devastating wind speeds, heavy rainfall, and storm surges cause widespread destruction to lives, infrastructure, and agricultural land, resulting in substantial loss of lives and properties. For example, the 1999 Orissa super cyclone and the 2008 Cyclone Nargis resulted in the loss of approximately 10,000 and 138,000 lives in the coastal regions of the Indian subcontinent [7, 8]. Furthermore, reports indicate that cyclones occurring in BoB have led to a tragic toll of over 0.75–1.23 million lives lost, impacting 61.6 million individuals, and causing economic damages estimated between $4.7 billion to $9.0

billion in the coastal states of Bangladesh [9]. The frequent formation of TCs over the BoB throughout the year, coupled with their rising destructiveness, has become a major concern in the Indian subcontinent in recent times [10, 11]. Accurate TC prediction is essential for minimizing fatalities and property damage. A reliable genesis potential index can be crucial for forecasting the formation and intensification of these storms.

Enhancing our comprehension of TCs' variations is of utmost importance both from scientific and societal standpoints, especially given the ongoing shifts in our climate. The advancement of computational capabilities has supported the potential of regional and global weather prediction models to simulate the intricate mesoscale phenomena observed during cyclogenesis [12-15]. Key parameters influencing TC development include three thermodynamic factors—elevated Sea Surface Temperature (SST), increased mid-tropospheric relative humidity, and conditional instability—as well as three dynamic attributes—diminished VWS, notable Coriolis parameter, and heightened low-level Relative Vorticity [3, 16]. Nonetheless, even when all these prerequisites are met, the spontaneous emergence of a TC is not a given assumption [17, 18]. Beyond the aforementioned conditions, an additional imperative factor for cyclogenesis is the presence of a finite amplitude disturbance feature in waves with wavelengths ranging from 1,000 to 3,000 km, acting as a catalytic seed [19]. Consequently, cyclogenesis can be contemplated as a stochastic process influenced by environmental stimuli, hinging on numerous critical criteria, as well as weather-induced perturbations, primarily stemming from transient tropical disturbances over short time spans [20].

TCs form over warmer areas in tropical oceans and develop under favorable environmental conditions [21]. Cyclones are most likely to form in the late summer and early autumn when SSTs are at their highest [22]. Raymond *et al.* hypothesized that a cold and warm core over the lower and mid-troposphere can contribute to the development of a thermodynamically conducive environment that encourages frequent deep convection at lower levels, putting the 'top-down' mechanism into perspective [23]. The rise in SST and water vapor offers additional energy to storms, therefore when suitable conditions exist, the increased SST and specific humidity promote more severe storms [11]. A moist mesoscale vortex in the mid-troposphere is considered the contributory factor to TC formation [24-27]. The transportation and convergence of atmospheric moisture have a substantial influence on the distribution of latent heat in TCs [28]. The discharge of latent heat resulting from the condensation of water vapor serves as the primary fuel for TCs [29]. Despite low and mid-level vortices, the disturbance can't develop into a TC due to the low water vapor contents [30]. TC formation and intensification events are significantly hampered by high VWS magnitudes between 200 and 850 hPa levels [31, 32].

Over the past several decades, numerous researchers have continued to develop various techniques and methods for forecasting the genesis, intensification, and other features of TCs using various numerical weather prediction models [33-45]. Sousounis *et al.* used the WRF, RUC, ETA, and MM5 models to examine several precipitation events. They concluded that the WRF model can develop physically precise and reliable fine-scale structures more effectively than any other model [46-48]. The WRF model performs reasonably well in forecasting the formation and intensification events of TCs over the BoB [49]. Higher grid resolution in numerical weather prediction models represents better regional and small-scale dynamics, as well as increases the potential to improve TC intensity forecasting [50-53]. Based on 65 sensitivity analyses of five Severe Cyclonic Storms (SCS), Srinivas *et al*. concluded that the combination of Kain-Fritsch (KF) convection, LIN explicit microphysics schemes, Yonsei University (YSU) planetary boundary layer, and NOAH land surface schemes offer a comparatively better realistic prediction of TC intensification [54].

Understanding the mechanism that contributes to the formation of TCs is one of the main challenges in TC prediction. Although recent advancements in numerical modeling with improved physics and resolution have shown significant improvements in TC prediction, they often fail to capture important aspects of the cyclogenesis phase [24, 55, 56]. The widely used strategy in understanding the developing and non-developing systems during the cyclogenesis stage is known as the Genesis Potential Parameter [55, 57-63]. McBride and Zehr studied the dynamic and thermodynamic characteristics of tropical disturbances in the western North Pacific. They proposed a daily Genesis Potential Parameter (GPPI), which is determined as the vorticity difference between 900 and 200 hPa levels. The study suggests that this parameter could be applied to differentiate between developing and non-developing tropical disturbances [24]. Roy Bhomik found that a low-pressure system with GPPI value 10×10^{-12} has the potential to intensify into a hurricane [55]. DeMaria *et al.* investigated the potential of cyclogenesis between Africa and the Caribbean islands in the North Atlantic. They introduced a genesis parameter as the product of mean vertical wind shear, instability, and moisture factors. This parameter can be used to analyze cyclogenesis as well as interseason variability in TC formation over this region [64].

Every year, the BoB has a significant number of low-pressure systems, but only a small number of these systems intensify into disastrous storms. To minimize the catastrophe of severe storms, accurate weather forecasts and effective disaster management and mitigation strategies are essential. A suitable GPPI that could indicate early in the system's development whether it has the potential to intensify into a cyclonic storm can be very crucial for early warning systems and disaster preparedness. Kotal *et al.* proposed a GPPI that contains

both dynamic and thermodynamic parameters to distinguish between developing and non-developing low-pressure systems over the Indian Ocean [62]. They demonstrated that this approach can reliably predict most of the developing and non-developing cases. However, the GPPI of a significant number of depression cases showed enough potential for intensification, but no one there ultimately developed [62]. GPPI values also demonstrated no discernible difference between developing and non-developing systems in the early stages of the system [55]. These limitations motivate us to develop a suitable RGPPI to predict TC formation and intensification events over the BoB. The main objective of this study is to develop the RGPPI and verify whether it can provide insight into the suitability of the existing environment for cyclone formation. It is also studied which parameters play the most crucial role in TC development over the BoB. It is expected that the proposed technique may provide more realistic predictions for cyclonic system formation and intensification. A diagnostic study of the parameters governing TC formation will also be crucial in understanding their dynamics. The RGPPI approach, with a deeper understanding of each parameter, may collectively offer more realistic predictions for the formation and intensification of the cyclonic systems.

2. Description of Cyclonic Systems

The following subsection offers a summary of the weather conditions linked to the cyclonic systems examined in this study.

2.1 Extremely Severe Cyclonic Storm (ESCS) Fani

Extremely Severe Cyclonic Storm (ESCS) Fani originated from a Low-pressure Area (LPA) that developed in the early hours of April 25, 2019, over the EIO and adjacent southeastern BoB (approximately 2.70°N and 88.70°E) [65, 66, 67, 68]. The system deepened into a Depression (D) across the identical regions around 0300 UTC of 26 April. Proceeding northwest, it became a Deep Depression (DD) and subsequently intensified into a CS, Fani, around the morning and midday of 27 April, respectively [65, 66, 67, 68]. Continuing its movement to the northwest, it intensified into a SCS on the evening of 27 April and then turned into a Very Severe Cyclonic Storm (VSCS) across the same area in the early morning of 30 April. It subsequently proceeded west-northwestwards and concentrated into an ESCS across west-central and the southwest BoB at 0000 UTC on 30 April. It reached the highest severity of 115 knots from the evening of 2 May till the early hours of 3 May. After dropping a few strengths, it crossed the Odisha coast near Puri at approximately 0300 UTC of 3 May with a Maximum Sustained Wind Speed (MSWS) of 175–185 kmph [65, 66, 67, 68]. The total accumulated cyclone energy and power dissipation index for the ESCS Fani was found to be higher compared to the long-term average (1972–2017) [69]. The overall system life duration was 204 hours from D to D. It had one of the largest tracks, with a total track length of 3030 km.

2.2 VSCS Yaas

The VSCS Yaas was formed from an LPA that occurred over the west-central BoB at 0300 UTC of 2 May 2021. The LPA developed into a well-marked LPA throughout the same region at approximately 0900 UTC on the same day [49, 70, 71, 72]. Under the suitable climatological situation, the system intensified into a D over the same region at about noon of 23 May [49, 71]. It strengthened into a DD and then into a CS, Yaas, over the same region during the midnight of 23 May and the early morning of 24 May, respectively, after proceeding northwestwards. Continuing its movement north-northwestwards, it deepened into a SCS and VSCS around 1800 UTC of 24 May and 1200 UTC of 25 May, respectively. It reached the Odisha coast close to latitude 21.35°N and longitude 86.95°E as a VSCS with MSWS of 75 kts to 85 kts [49, 70, 71, 72]. The highest intensity of the CS was 75 kts to 85 kts. The cyclone's trajectory was 703 km long [71]. From D to D, the total lifetime of the system was 114 hours.

2.3 CS Burevi

The CS Burevi formed as a low-pressure system in the equatorial easterly wave across the South Andaman Sea and neighboring portions of the Southeast BoB and EIO on 28 November 2020 [73, 74, 75, 76]. On 29 November, it became a well-defined LPA over the same region. It moved over the Southeast BoB on 30 November, at 0000 UTC, and strengthened into a D. It concentrated into a DD early on 1 December, over the Southwest and neighboring Southeast BoB as it proceeded almost westward. Subsequently, on 1 December, in the evening (1200 UTC), it proceeded west-northwestward and developed into CS "Burevi" over Southwest BoB [75, 76]. On 2 December, between 1700 and 1800 UTC, it crossed Sri Lanka's coast near the north of Trincomalee in keeping with its west-northwestward movement [75, 76]. it continued to move west-northwestwards and degraded into a DD over the Pamban area in the evening (1200 UTC) of 3 December. The movement of the system declined considerably, and it was therefore almost stationary over through the Gulf of Mannar close to the coast of Ramanathapuram district for almost 18 hours. On 4 and 5 December, it weakened into a D and subsequently into an LPA over the same region [74].

2.4 DD (6–9 December 2017)

The DD (6–9 December 2017) developed from a LPA over the Malay Peninsula and the surrounding Andaman Sea on the morning of 30 November 2017 [77]. It was a well-defined low-pressure system across the southern Andaman Sea and the adjacent Malacca Strait on 1 December. After continuing to make progress toward the southeast BoB and the surrounding region until 5

December. It developed into a D over the same region on 6 December. Moving north-northwestward, it deepened into a DD over the central BoB in the early morning of the 8 December [77]. During that day's night, it proceeded almost northward and degraded into D over western BoB. On 9 December, it kept turning in a north-northeasterly direction in the morning and diminished into a LPA over Northwest BoB in the evening. It is important to note that the system deteriorated over the sea. Throughout its 51-hour lifetime, the system caused severe to extremely severe rainfall across north coastal Andhra Pradesh and coastal Odisha[77].

3. Methodology

The Weather Research and Forecasting (WRF) Model stands as a sophisticated mesoscale numerical weather prediction system designed for both atmospheric investigation and practical forecasting applications. Through its incorporation of multiple physics approaches and its effectiveness across various uses, the WRF model surpasses many other numerical operational models available for simulating the atmosphere and conducting meteorological studies, solidifying its position as the most widely employed numerical weather prediction model worldwide. The WRF-ARW model can generate simulations based on real-world atmospheric conditions (observations and analysis) as well as idealized configurations. The WRF ARW model version 4.3.1 has been applied in this present study. The WRF-ARW model has been executed on a single domain with a horizontal resolution of 10 kilometers to simulate the formation and intensification procedures of the selected systems. The central point of the domain has been used as 5°N & 87°E; 16.5°N & 87.5°E; 6.0°N & 86.0°E, and 13.0°N & 86.0°E respectively. For ESCS Fani, the total number of grid points in both the west-east and north-south directions was 280. The total number of grid points over the selected domain for VSCS Yaas, CS Burevi, and the DD case was 170, 180, and 170, respectively, both in the west-east and north-south directions. The map projection used in this study is Mercator. This study uses the Kain-Fritsch (new Eta) scheme for cumulus parameterization [78], the Kessler scheme for microphysics [79], and the Yonsei University (YSU) scheme for the planetary boundary layer [80]. The physics parameterization schemes used in the present study are the Revised MM5 scheme for surface layer physics [81], the Unified Noah LSM scheme for the land-surface model [82], the Dudhia scheme for short-wave radiation [83], and the RRTM scheme for long-wave radiation [84].

The National Center for Environmental Prediction (NCEP) FNL (Final) operational global analysis and forecast data (0.25º × 0.25º) from the Global Data Assimilation System (GDAS) organized operationally every six hours have been used as the initial and lateral boundary conditions in the present work. The model simulated Minimum Central Pressure (MCP) and MSWS outcomes have been compared with the India Meteorological Department (IMD) observations for all cases. The computed RGPPI pattern has been compared with the GPPI pattern of Kotal *et al.* [62]. The observations of the other simulated parameters are currently unavailable to the authors.

4. Results and Discussion

Four cyclonic systems of varying intensities across the BoB between 2017 - 2021 have been considered in the current study. The following section offers a diagnostic analysis of several meteorological parameters connected with the RGPPI index in understanding the formation and development processes of cyclonic systems.

4.1 Analysis of Mean Sea Level Pressure

A significant decrease in sea level pressure, forming a LPA, is a crucial phase in the formation of weather disturbances that might turn into a TC under suitable environmental conditions. The model simulated Mean Sea Level Pressure (MSLP) distribution of the selected cyclonic systems Fani, Yaas, Burevi, and DD cases are presented in Fig. 1 (a – l) respectively. According to the simulated MSLP distribution of ESCS Fani, a LPA is formed at 0300 UTC of 25 April over the east EIO and its adjacent southeastern BoB for the 72-hour simulation based on 0000 UTC of 24 April 2019. The determined LPA position and timing closely correspond to the observations. The center of cyclonic system Fani is predicted to be at different positions in various simulations: 4.68º N/87.40º E for 72 hours, 5.59º N/86.04º E for 48 hours, and 4.38º N/89.41º E for 24 hours. The simulated MCP for the ESCS Fani during the genesis stage at 0000 UTC on April 27 was around 965 hPa for the 72-hour simulation, 975 hPa for the 48-hour simulation, and 990 hPa for the 24-hour simulation.

A LPA is simulated to develop throughout the west-central section of the BoB by 2200 UTC on May 22, according to the 72-hour simulation for the VSCS Yaas. By 0000 UTC on May 24, the system's simulated positions are approximately 17.77ºN/89ºE for 72 hours, 17.2ºN/90.2ºE for 48 hours, and 16.5ºN/88.97ºE for 24 hours. The predicted MCP is determined around 965 hPa for the 72-hour simulation, 975 hPa for the 48-hour simulation, and 984 hPa for the 24-hour simulation.

CS Burevi originated from a low-pressure system within the equatorial easterly wave, spanning the South Andaman Sea and adjacent areas of the Southeast BoB and the EIO on November 28, 2020[73, 74, 75, 76]. According to the simulations, a low-pressure system formed throughout the South Andaman Sea and neighboring regions in the early morning of 28 November. Since its formation, the system has been observed recurving predominantly westward. Around November 30, the system exhibited a small curvature over the southern BoB, which was consistent with observations. 975, 981, and 1000 hPa are the simulated MCP of the system for 72-,

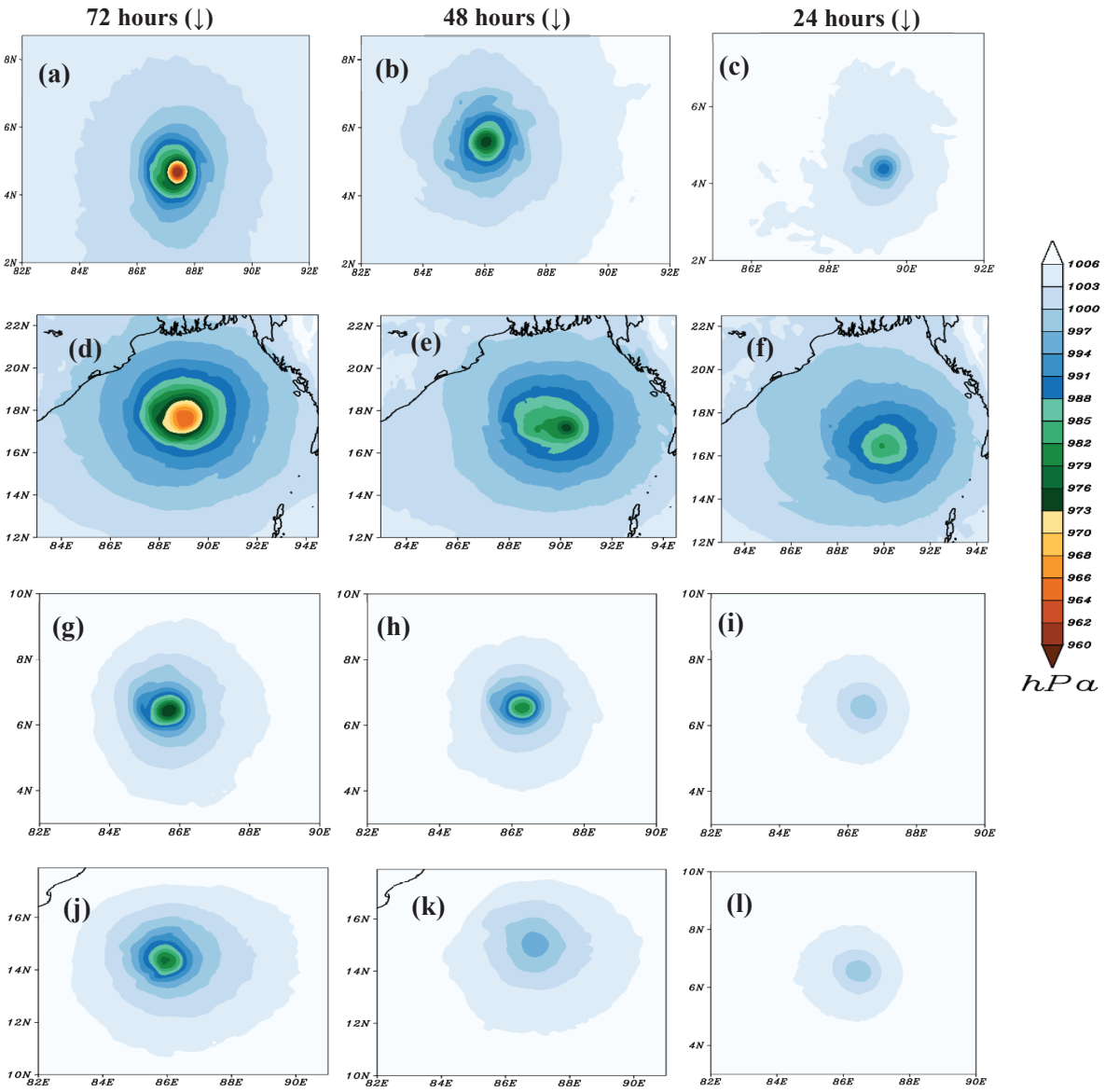

Fig. 1: The simulated MSLP distribution of ESCS Fani (a–c) valid for 0000 UTC of 27 April 2019, VSCS Yaas (d–f) valid for 0000 UTC of 24 May 2021, CS Burevi (g–i) valid for 0000 UTC of 1 December 2021, and DD (j–l) valid for 0000 UTC of 8 December 2017 respectively.

48-, and 24-hour lead time simulations.

The system's center location and MCP have shown slight variations across several simulations. The MCPs continually decrease over time, suggesting the system is organized with a pressure gradient, indicating potential for strengthening. However, the model tends to predict significantly lower MCPs, indicating more severe conditions than observed. In the DD case, the simulated MCPs are higher compared to other cases. The pressure differences within the simulated system might indicate potential storm categories. Despite some inaccuracies, the model generally performs well in simulating the MSLP distribution.

4.2 Wind Flow Analysis

The horizontal wind flow distribution (m s^{-1}) at the 850 hPa level for the cyclones Fani, Yaas, Burevi, and DD case has been shown for 72-hour, 48-hour, and 24-hour simulations in Fig. 2 (a - l). The presence of dominant cyclonic flow in the Northern Hemisphere is a key factor influencing the formation and development of TCs [79-81]. The wind flow analysis at the 850 hPa level for the ESCS Fani reveals a strong cyclonic circulation across the simulated region, with a well-organized center zone near the equator and surrounding regions in the BoB. The model-predicted system is almost organized for the 24-hour simulation, but the wind speed is lower compared to

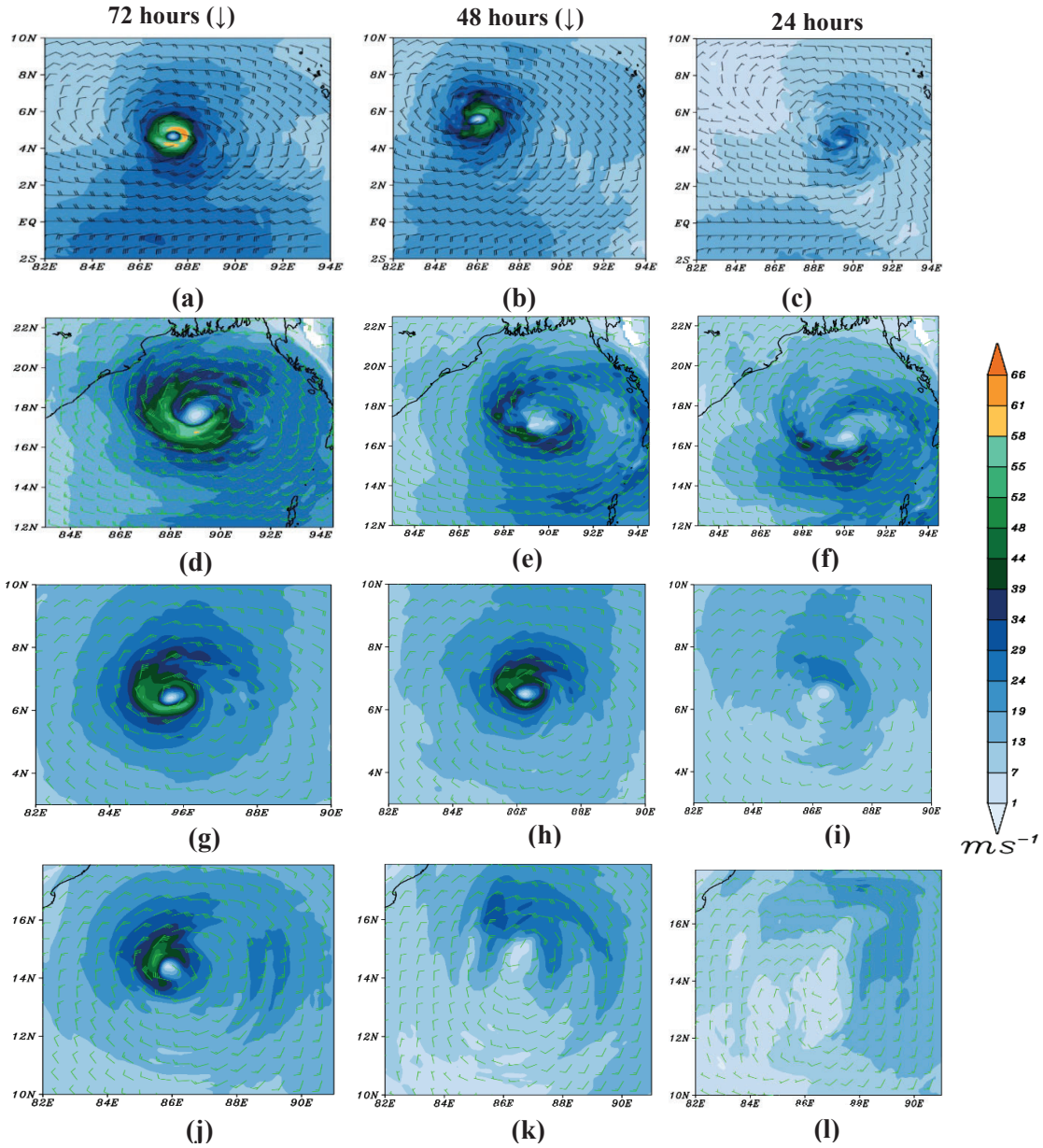

Fig. 2: The simulated wind flow (m s^{-1}) distribution at 850 hPa level of ESCS Fani (a–c) valid for 0000 UTC of 27 April 2019, VSCS Yaas (d–f) valid for 0000 UTC of 24 May 2021, CS Burevi (g–i) valid for 0000 UTC of 1 December 2021, DD (j–l) valid for 0000 UTC of 8 December 2017 respectively.

the 72- and 48-hour simulations. During the genesis stage of ESCS Fani, the model simulated MSWS at the 850 hPa level is determined to be 65, 50, and 35 m s^{-1} for lead times of 72, 48, and 24 hours respectively, indicating a decrease in wind speed as the lead time reduced, despite the system being nearly organized in the 24-hour simulation. A cyclonic circulation is demonstrated over the simulated region in all cases according to the model's simulated results. In the cyclonic systems Yaas and Burevi, the core of the system, known as the zone of convergence, is well-structured in 72- and 48-hour simulations. This convergence zone plays a crucial role in absorbing heat and energy from the sea surface, thereby contributing to the system's favorable environment for development. For all cases, the model simulates a well-structured convergence zone at the 72-hour lead time, but as the lead time reduces, the predicted central region becomes slightly disorganized compared to outcomes of higher lead time simulations. Specifically, in the DD case, while the center is organized in the 72-hour simulations, it appears more scattered in the 24-hour simulations.

The model simulates that the MSWS of all systems are located over their respective eyewalls. For VSCS Yaas, the model-predicted MSWS values are determined 55, 45, and 40 m s^{-1} for 72-hour, 48-hour, and 24-hour lead time simulations respectively. For CS Burevi, the simulated MSWS values are 55, 45, and 27 m s^{-1} for the same lead times.

In the case of DD, the model predicts MSWS values of 50, 30, and 20 m s^{-1} respectively for the 72-hour, 48-hour,

and 24-hour lead time simulations during the genesis stage. At the 200 hPa level, a cyclonic circulation is found in all events, but it lacks a well-defined structure. Additionally, a divergence zone is observed at this level (Fig. not shown). During the genesis stage, a well-organized zone is identified up to the 500 hPa level, but at 200 hPa, the divergence zone is prominent. Despite the disorganized nature of the divergence zone in the first three cases, it tends to develop into a convergence zone, indicating the possibility of more cyclonic rotation. However, in the DD case, the system's cyclonic circulation is comparably feeble, and the center appears scattered at the 200 hPa level, which may indicate the system's degradation.

4.3 Sea Surface Temperature Distribution Analysis

TC formation is significantly influenced by the temperature of the underlying ocean, particularly the thermal energy within the upper 60 meters (about 200 feet) of ocean waters. TC formation typically requires a water temperature higher than 26ºC [3, 16]. Warm SSTs ranging from 30–31ºC were recorded throughout the BoB approximately a week before the formation of ESCS Fani, spanning from 19-25 April 2019 [69, 88]. ESCS Fani was noted to have the highest mean SST of 30.4°C before the genesis stage compared to any other cyclone forming over the BoB during April between 1990-2019[88]. The simulated horizontal and vertical cross-section of the SST of cyclonic systems Fani, Yaas, Burevi, and a DD case has been analyzed in this study. The model-predicted SST distribution of ESCS Fani at a 2-meter height reveals that the temperature of the simulated region ranges between 26.35-30.35°C, except for some small areas just outside the center (Fig. 3 (a–c)). During the genesis stage of VSCS Yaas, the model-predicted SSTs are found to be ≥ 27°C, 29°C, and 29°C for the 72-hour, 48-hour, and 24-hour simulations, respectively. For CS Burevi, the simulated maximum SST ranges from approximately 28–30°C, 28–31°C, and 28–32°C for the 72-hour, 48-hour, and 24-hour lead time simulations. In the case of DD, the simulated SST is consistently around 28–32°C for all simulations. The cyclonic systems Fani and Yaas show higher temperatures across the simulated regions compared to cyclonic systems Burevi and the DD case. This warmer SST supplies the required fuel for the system's growth and aids in its intensification[16, 69]. However, in the DD case, the SST in the northwest sector of the simulated region is significantly lower than on the other sides, potentially impacting the system's development (Fig. 3 (j – l)).

The vertical cross-section of temperature distributions, exhibited using the latitude of the system's center, indicates a warm-core system in the temperature field extending from the system center to the mid-tropospheric level. This warm-core structure may be a result of the system's downward compensation. The 24-hour simulations for cyclonic systems Fani, Yaas, and Burevi also exhibit the presence of a warm core. As this warm core matures and static stability develops over the inner core, conditions for frequent upward convection become less favorable, leading the storm to transition into a more stable state. These high SST and warm-core temperature systems are highly conducive to cyclone formation and intensification. However, in the case of DD, the presence of a warmed core appears to be absent according to 24-hour lead time simulations, indicating limitations that may impede the system's development.

4.4 Vertical Wind Shear Analysis

Environmental VWS is a crucial factor that may influence the formation, growth, and maintenance of cyclonic systems [32, 89, 90]. W. M. Gray's research highlighted that hurricanes are particularly sensitive to the east-west, or "zonal," component of wind shear, while the north-south, or "meridional," component had a negligible impact on these storms [3, 16]. From the analysis of VWS using the u-component of velocity between the (500 and 850) hPa levels and the (200 and 850) hPa levels (not shown in the Fig), it is found that the VWS value in the system center varies between 5-10 m s^{-1}. This indicates that at the system center, the wind is in an exceedingly calm state for the simulated cases. For ESCS Fani, the maximum VWS values are determined around 40, 30, and 30 m s^{-1} for the 72, 48, and 24-hour simulations respectively, between the 200 and 850 hPa levels. Similarly, for VSCS Yaas, the maximum sustained VWS values between these levels are found as around 30 m/s for all simulations. For CS Burevi, the simulated maximum VWS values are 40, 30, and 30 m $s^{-1}$for the 72-hour, 48-hour, and 24-hour simulations respectively. In the DD case, the VWS magnitudes are approximately 30 m s^{-1} for all lead time simulations.

The maximum VWS values for ESCS Fani are about 40, 30, and 30 $m\ s^{-1}$ for the 72, 48, and 24-hour simulations between the 200 and 850 hPa levels respectively. Similarly, for VSCS Yaas, the maximum sustained VWS values between these levels are approximately 30 m/s for all simulations. For CS Burevi, the simulated maximum VWS values are found around 40, 30, and 30 $m\ s^{-1}$ for the 72, 48, and 24-hour simulations respectively. In the DD case, the VWS magnitudes are determined as 30 $m\ s^{-1}$ for all lead time simulations.

These simulated VWS values are higher compared to the theoretically determined suitable VWS values. Higher VWS can potentially harm TCs by reducing the heat and moisture they require from the surrounding region, and it may also distort the TC structure by separating the top from the lower portion. Between the 500 and 850 hPa levels, the maximum values of VWS for the ESCS Fani are relatively low to moderate, around 15, 10, and 15 $m\ s^{-1}$ for the 72-, 48-, and 24-hour simulations, respectively in the surrounding areas of the system center.

For VSCS Yaas, the simulated VWS values are approximately 10, 10, and 15 $m\ s^{-1}$ for the 72-, 48-, and

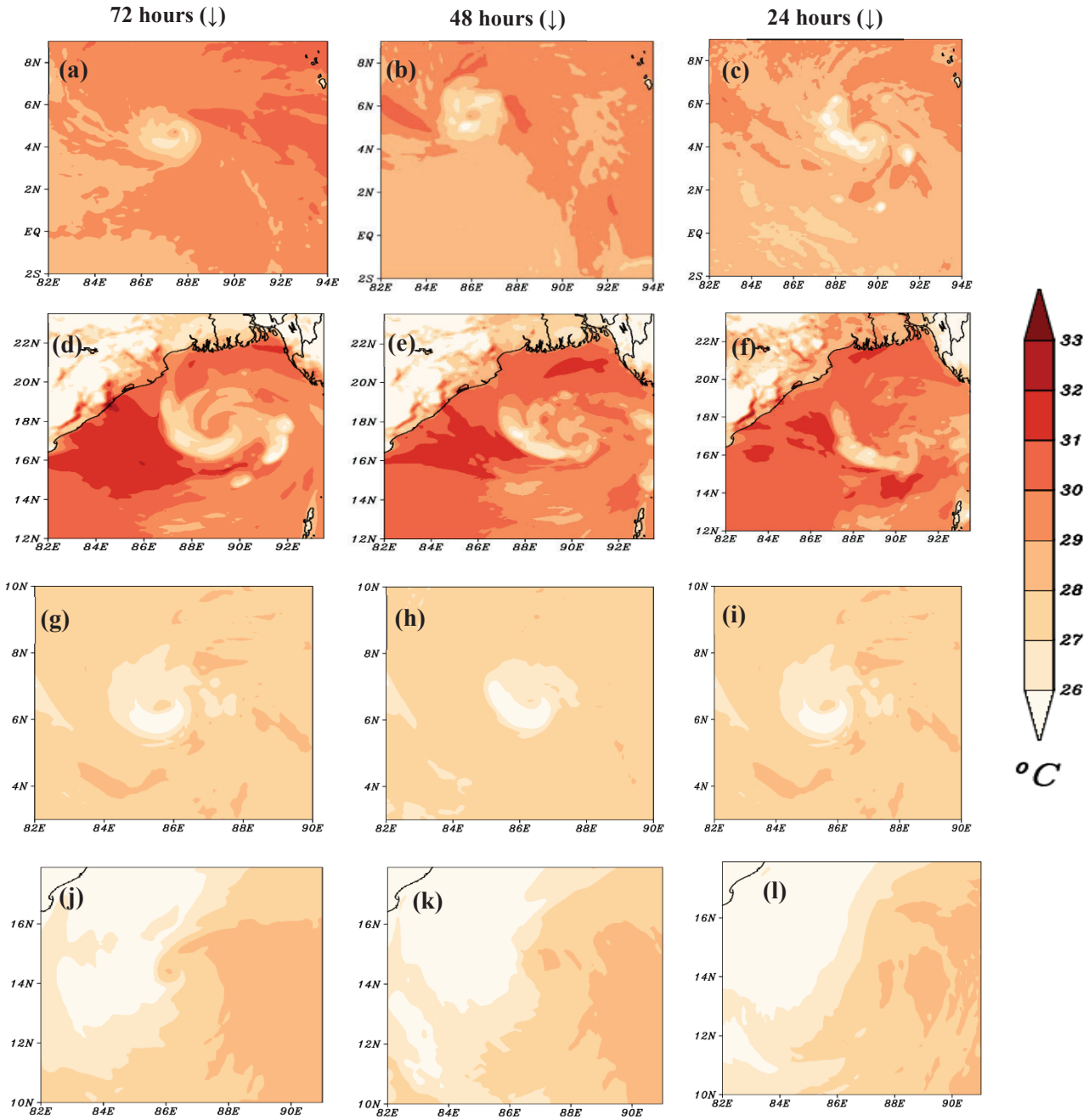

Fig. 3: The simulated temperature (□C) distribution of ESCS Fani (a–c) valid for 0000 UTC of 27 April 2019, VSCS Yaas (d–f) valid for 0000 UTC of 24 May 2021, CS Burevi (g–i) valid for 0000 UTC of 1 December 2021, and DD (j–l) valid for 0000 UTC of 8 December 2017 respectively.

24-hour simulations. Similarly, the maximum VWS values for CS Burevi are determined as 20, 15, and 12 $m\ s^{-1}$ the 72-, 48-, and 24-hour simulations. Similarly, the maximum VWS values for CS Burevi are determined as 20, 15, and 12 $m\ s^{-1}$ for the 72-, 48-, and 24-hour model runs respectively. In the case of DD, the VWS values are about 15, 10, and 9 $m\ s^{-1}$ respectively. Significantly, the VWS values decrease as the lead time of the simulations diminishes. These values for the simulated cyclonic systems are determined to be low to moderate for all simulations. Moderate VWS values in the lower troposphere may contribute to the development of cyclonic systems. However, in the DD case, the simulated VWS values are comparatively higher between the 200 and 850 hPa levels, which could be detrimental to system development. Furthermore, these higher VWS values prevailing over the upper troposphere may lead the systems in a recurving movement, causing the center to be displaced[91].

4.5 Relative Vorticity Analysis

TCs do not form spontaneously from random convection. They require a "seed" to govern the environment surrounding them. Positive vorticity, which indicates how air spins, is important for their formation, especially in regions near the equator where the Coriolis force is extremely low [92]. From the model simulated relative vorticity analysis at 850 *hPa* and 500 hPa levels, it is determined that both positive and negative vorticity are generated through the simulated regions. The predicted maximum positive vorticity is determined in the system's eyewall and it is found positive for each level. The maximum positive vorticity is about 160, 120, and 140 × 10^{-5} s^{-1} at 500 hPa level and 300, 250, and 210 × 10^{-5} s^{-1} at 850 *hPa* level for ESCS Fani. The highest positive vorticity for VSCS Yaas is predicted around 120, 150, and 120 × 10^{-5} s^{-1} at 500 hPa level and 200, 200, and 180 × 10^{-5} s^{-1} at 850 hPa level, respectively. 330, 335, and 110 × 10^{-5} s^{-1} and 140, 140, and 70 × 10^{-5} s^{-1} are the simulated RV at 850 and 500 hPa levels for the CS Burevi respectively. For the DD case, the simulated maximum RVs are determined approximately 265, 90, and 90 × 10^{-5} s^{-1} and 140, 120, and 50 × 10^{-5} s^{-1} at 850 and 500 hPa levels for 72, 48, and 24-hour simulations. It is also observed that the positive vorticity values have diminished as the distance from the system's center increases. RV is found to be positive up to 200 hPa level, indicating cyclonic circulation up to the upper-tropospheric level. This suggests that there's a significant pre-existing vortex up to the middle troposphere, which helps trigger strong updrafts from the lower troposphere during the system formation [27, 93, 94].

4.6 Relative Humidity Analysis

Relative humidity of the higher order in the low-to-middle troposphere plays a crucial role in the formation and intensification of TCs[3, 82]. The model's relative humidity analysis at 2m height shows a strong, consistent supply of moisture from the southwest, with values ranging from 80-100%. This moisture is crucial for triggering intense convective activity related to cyclonic systems. Relative humidity just above the center is relatively lower (around 70%) compared to its surroundings up to the mid-tropospheric level. However, vertically, relative humidity extends from 90-100% up to the mid-tropospheric level, indicating favorable conditions for cyclone intensification. High relative humidity, extending from the surface to the mid-troposphere, is concentrated around the center's periphery during the genesis stage, which is highly conducive to cyclone formation.

4.7 Revised Genesis Potential Parameter Index

The formation of TCs is closely linked to specific weather conditions. Key factors include low-level RV, mid-tropospheric relative humidity, mid-tropospheric instability, and VWS between 200 and 850 hPa. These parameters are crucial for the development of cyclonic systems. Kotal *et al.* [60] have calculated the GPPI using the following formula:

$$GPPI = \begin{cases} \dfrac{\zeta_{850} \times I \times P}{S} \text{ if } \zeta_{850} > 0, \mathrm{I} > 0, \text{and P} > 0 \\ 0 \text{ if } \zeta_{850} \leq 0 \text{ and P} \leq 0 \end{cases}$$

Here, ζ_{850} = low-level RV (10^{-5} s^{-1}) at 850 hPa level,
Mid − tropospheric relative humidity

$$p = \frac{|RH_{mean} - 40|}{30},$$

where RH_{mean} is the average relative humidity of 700 and 500 hPa level,
$S =$ VWS between 200 and 850 hPa level (m s^{-1}),
and Mid-tropospheric instability between 850 and 500 hPa levels, $I = (T_{850} - T_{500})\,℃$
It is recognized that The severity of cyclonic systems is determined by the MCP in the core region of the storm. MCP and MSWS are vital factors used to categorize cyclones [96, 97]. Using these, the RGPPI can be formulated as:

$$RGPPI = \begin{cases} \dfrac{\zeta_{850} \times I \times P \times M \times V}{S \times 1000} \text{ if } \zeta_{850}, P, V, and\ M > 0, \\ = 0 \text{ if } \zeta_{850}, P, V, and\ M \leq 0 \end{cases}$$

Here, M = (1013−MCP) hPa, V = wind speed at 850 hPa level (m s^{-1}).

This section compares the RGPPI with various developing and non-developing low-pressure systems to establish its threshold value throughout the BoB. Recent cyclonic systems like ESCS Fani, VSCS Yaas, CS Burevi, and DD cases are analyzed using the RGPPI technique. Data from NCEP re-analysis, available at a 0.25° latitude-longitude grid, is utilized to simulate these events. The analysis shows that the average RGPPI values for developing systems exceed 30.0, while those for non-developing systems are below 30.0. Table 1 presents the average RGPPI values of the simulated systems, and Fig. 4 (a-l) graphically illustrates the calculated GPPI and RGPPI.

For ESCS Fani, the mean RGPPI values are 567, 272, and 118 for 72-hour, 48-hour, and 24-hour simulations, respectively. These values significantly exceed the threshold of 30, indicating a high potential for severe intensification of the system. The variation in the calculated GPPI values over time show no clear trend for the 72-hour simulation, suggesting no distinct indication of the system's severity increasing or decreasing. In the 48-hour simulation, GPPI increases until 0600 UTC of April 26, then starts declining. In the 24-hour simulation, GPPI shows a downward trend overall. However, the last 12 hours of the simulation show an upward pattern,

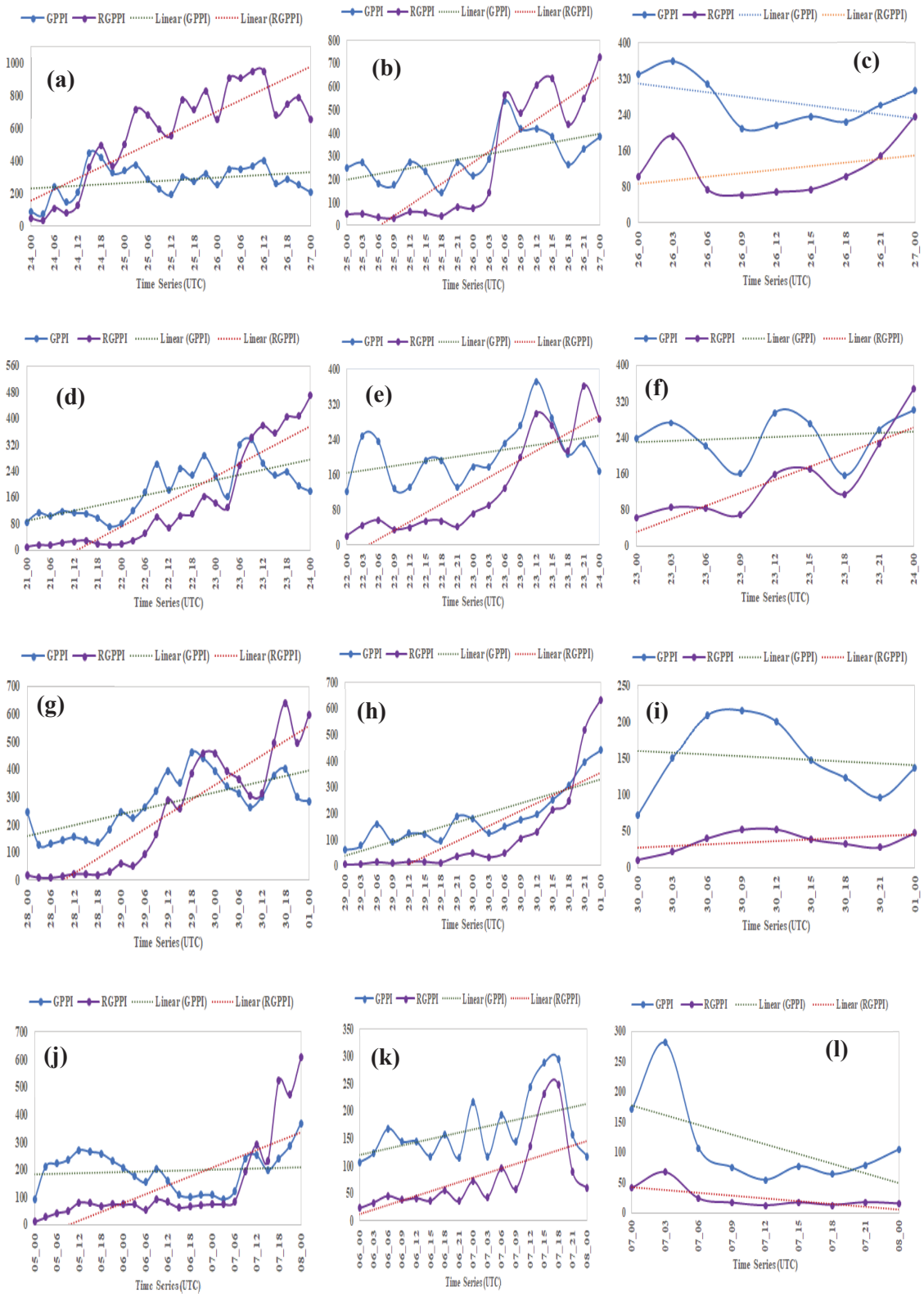

Fig. 4: Time series of GPPI and RGPPI of ESCS Fani (a–c), VSCS Yaas (d–f), CS Burevi (g–i), and DD (j–l) valid for 72-, 48-, and 24-hour simulations respectively

suggesting favorable conditions for system intensification. However, the last 12 hours of the simulation show an upward pattern, suggesting favorable conditions for system intensification. In contrast, RGPPI consistently shows an increasing trend over the time series for all simulations, clearly indicating system development. For VSCS Yaas, both GPPI and RGPPI show an increasing trend, suggesting cyclone formation. The sharp rise in

RGPPI offers a clearer insight into the system's potential severity compared to GPPI. The average RGPPI values for the 72, 48, and 24-hour simulations are 147, 134, and 146 respectively. These values indicate favorable atmospheric conditions for the system's development. The GPPI and RGPPI for the CS Burevi case demonstrate a rising tendency for both 72 and 48-hour lead time simulations. The mean RGPPI values are 238 and 123 for 72 and 48-hour simulations respectively. These RGPPI values are significantly higher than the threshold value. For 24-hour simulation, the GPPI generates slightly declining trends, whereas the RGPPI provides slowly increasing patterns. For the 24-hour lead time simulation, the RGPPI value is 36. The RGPPI value found in the 24-hour simulation is lower than the RGPPI values calculated in the 48 and 72-hour simulations, but it also exceeds the threshold value. The development of cyclones with relatively low intensity can be suggested by the average lower RGPPI values and the corresponding rising trend.

Table 1. Average RGPPI value of the simulated cases

Event	Lead time (hour)			Threshold Value
	72	48	24	
ESCS Fani	567	272	118	30
VSCS Yaas	147	134	146	
CS Burevi	238	123	36	
DD	142	78	25	

For the DD case, the average RGPPI values are 142, 78, and 25 for 72, 48, and 24-hour lead time simulations respectively. Both GPPI and RGPPI exhibit a rising trend for the 72-hour simulation. In the 48-hour simulation, both indices rise until 1800 UTC of July 7, but then decline significantly over the last six hours. This drop may be attributed to a significant decrease in RV at the 850 hPa level during that period. Both GPPI and RGPPI show a declining tendency for simulations over 24 hours. The downward trend, coupled with a relatively low mean RGPPI value (25), suggests the potential degradation of the cyclonic system. It's worth noting that the RGPPI value for the 72-hour simulation might be overestimated, as the model tends to intensify the system in the genesis simulations with longer lead times [49, 53, 98, 99].

Table 2 displays the simulated average values of M, V, I, ζ_{850} , and S. Figures 5-7 illustrate graphical representations of the average values and time series of these parameters for all simulations, respectively. Through statistical analysis of various environmental parameters associated with RGPPI, it's revealed that mid-tropospheric instability, relative humidity, and 850-hPa vorticity are the most influential factors in TC genesis over the BoB.

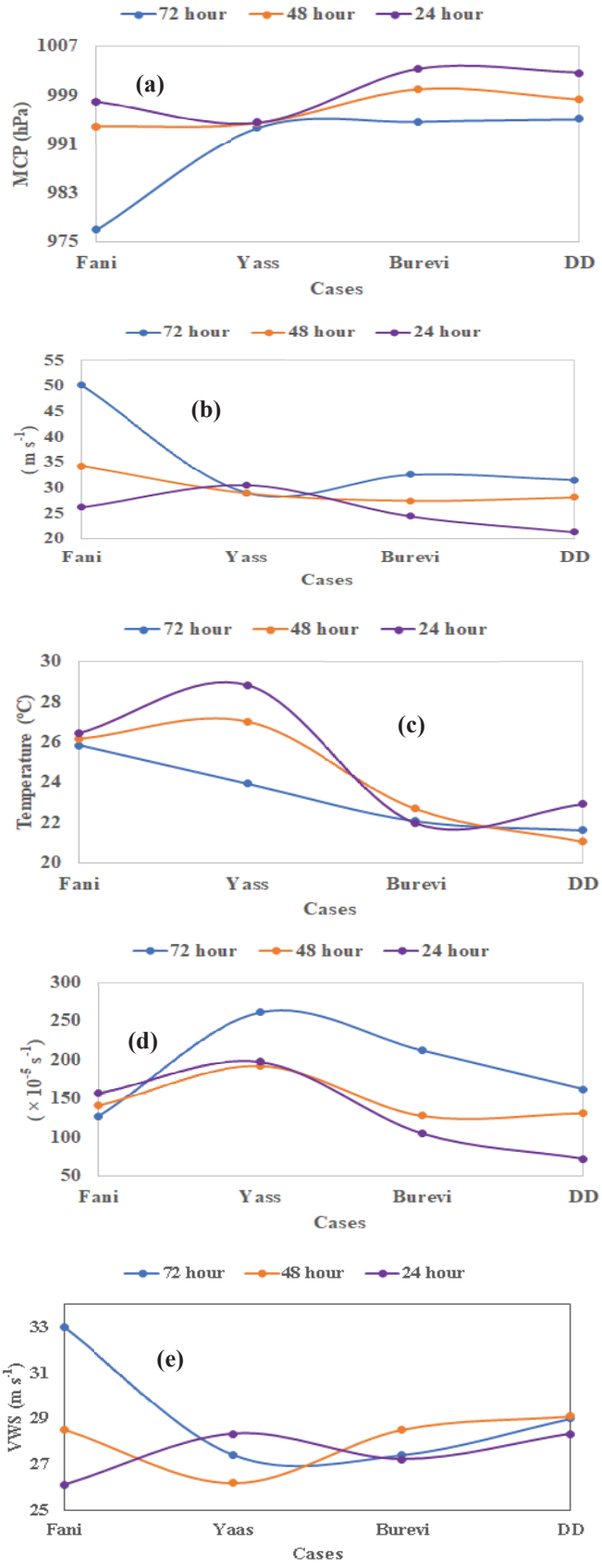

Fig. 5: Graphical representation of the simulated average values of M, V, I, ζ_{850}, and S for all simulations respectively.

Table 2. Simulated average values of M, V, I, ζ_{850}, and S for all simulations

Case	Lead time (hour)	M (hPa)	V (m s^{-1})	ζ_{850} $\times 10^{-5} s^{-1}$	I (°C)	S (m s^{-1})
Fani	72	976.92	50.12	127.20	25.82	33
	48	993.88	34.29	141.76	26.14	28.53
	24	998	26.22	157.78	26.44	26.11
Yaas	72	993.64	29.08	261.20	23.92	27.4
	48	994.38	29.00	192.35	27.00	26.18
	24	994.55	30.56	197.78	28.83	28.33
Burevi	72	994.68	32.60	212.00	22.07	27.4
	48	999.94	27.53	128.24	22.67	28.52
	24	1003.27	24.44	105.00	21.96	27.22
DD	72	995.08	31.56	162.00	21.61	29
	48	998.24	28.18	131.76	21.03	29.12
	24	1002.67	21.33	72.22	22.91	28.33

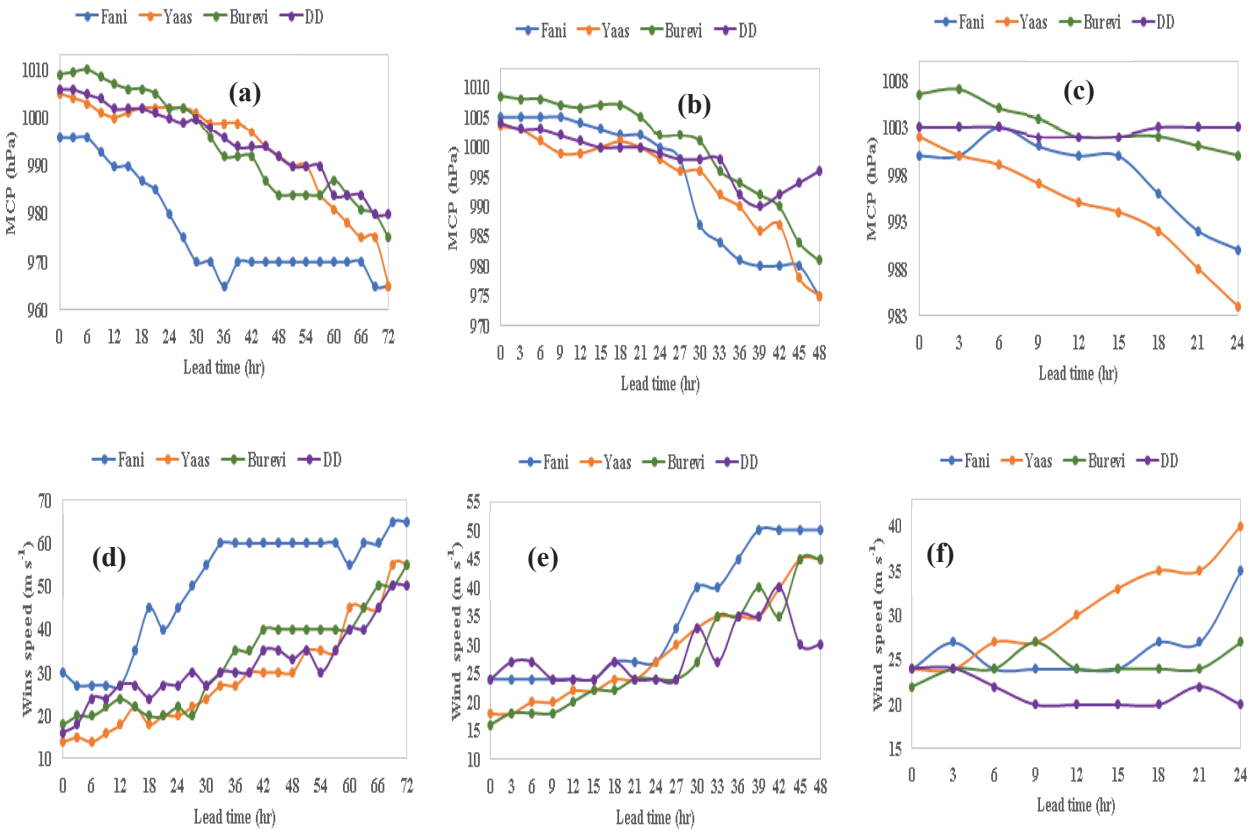

Fig. 6: Time series of simulated MCP (a–c) and MSWS (d–f) of the cyclonic systems Fani, Yass, Burevi, and DD case for all simulations

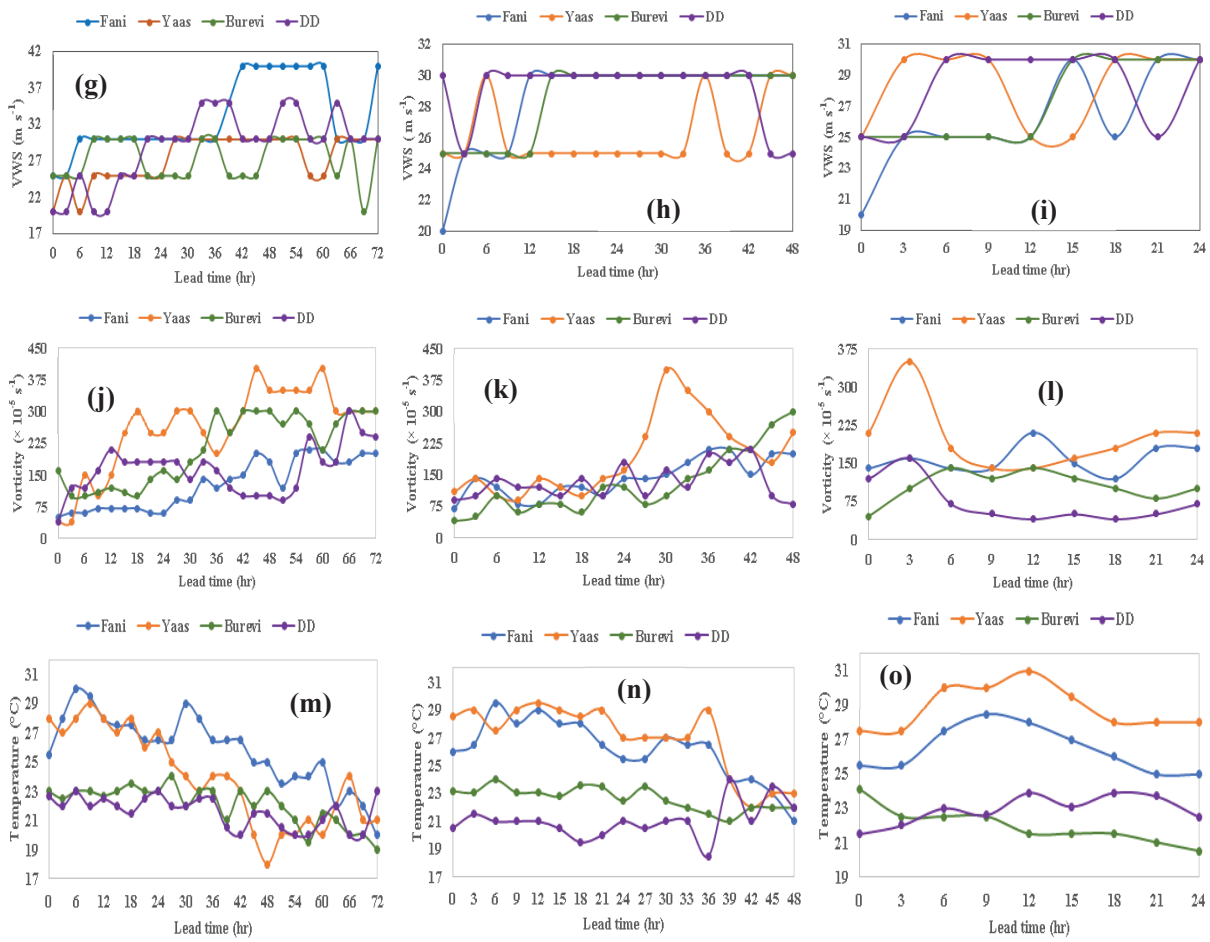

Fig. 7: Time series of simulated VWS (g–i), RV at 850 hPa level (j–l), and mid-tropospheric instability (m–o) of the cyclonic systems Fani, Yass, Burevi, and DD case for all simulations.

Mid-tropospheric instability, 850-hPa level relative vorticity, MCP, and V are deemed suitable for the development of cyclonic system Fani. Despite higher-than-ideal vertical wind shear, Fani concentrated and gradually developed into an ESCS due to substantial support from relative vorticity, relative humidity, and mid-tropospheric instability. For the cyclonic system Yaas, an average VWS of 26-28 $m\,s^{-1}$ is determined for all simulations. Despite the high VWS, other conditions, particularly high mid-tropospheric instability, and substantial relative vorticity, contributed to the development of VSCS Yaas. Strong mid-tropospheric instability may act as a buffer, reducing VWS and allowing the storm's core to remain vertically aligned, aiding storm organization and intensification [17, 19, 100]. Thus, TC development over the BoB can be significantly influenced by comparatively higher RV and mid-tropospheric instability, even in the presence of strong VWS. These factors play crucial roles in organizing and intensifying cyclonic systems, highlighting the complex interplay between various atmospheric conditions in the genesis and development of TCs over the BoB.

In the case of CS Burevi, all mentioned parameters, including VWS, are relatively weaker compared to cyclonic systems Fani and Yaas. Despite their comparative weakness, the combination of these factors is sufficient to support the development of the cyclonic systems Fani and Yaas. Despite their comparative weakness, the combination of these factors is sufficient to Burevi. The RV at the 850 hPa level and mid-tropospheric instability for CS Burevi are in the range of 105–262 × × $10^{-5}\,s^{-1}$ and 22–23ºC, respectively. Despite the presence of high VWS around 27-29 $m\,s^{-1}$, the severity is influenced by the combination of high RV and relatively low mid-tropospheric stability. Since the required mid-tropospheric instability and RV are relatively modest, the system could still intensify into a lower-category cyclone despite substantial VWS in the upper troposphere. For the DD case, mid-tropospheric instability and RV are relatively weak, while VWS is comparatively larger compared to the theoretically ideal value. This scenario raises the possibility that these environmental factors could lead to the degradation of the system. Furthermore, the outcomes indicate that VWS plays a negligible positive contribution to the development of the mentioned cyclonic systems in the presence of strong RV and mid-tropospheric instability. This finding is consistent with previous observations[101, 102].

TC activity over the BoB shows a strong correlation with the RGPPI. Realistic predictions have been made between

24 and 48 hours before the event, and notably, no system detection has failed using this parameter. This indicates that the RGPPI is crucial in assessing the potential of a TC in its early phase. Such information would be highly beneficial to operational forecasters, providing them with valuable insights for improved forecasting accuracy and early warning systems.

5. Validation of Simulation Results

The comparison between simulated results and observations for all simulations is presented in Tables 3, 4, and 5. At the genesis stage, the simulated MCP of ESCS Fani is around 961, 975, and 989 hPa for the 72-, 48-, and 24 simulations, respectively (Table 3) However, the Estimated Central Pressure (ECP) according to the IMD report is 997 hPa[68]. The corresponding absolute errors are 2.52, 1.52, and 0.61% respectively. The model simulated MSWS of ESCS Fani is noted as approximately 61, 50, and 40 $m\,s^{-1}$ valid for 72, 48, and 24-hour simulations valid at 0000 UTC of 27 April 2019 respectively while the estimated MSWS is 15.36 $m\,s^{-1}$ according to IMD report [70]. The computed errors are 37.5, 27.5, and 22.5 $m\,s^{-1}$, respectively. Comparatively, the simulated MCP errors for the Fani, Yaas, Burevi, and DD cases are minimum for the 24-hour simulation, determined to be 7, 6, 0, and 1 hPa, respectively, in comparison to the observations[68, 70-72]. The observed SST of Fani, Yaas, Burevi, and DD cases are 30-31, 30-31, 29-30, and 29-30ºC respectively [63, 65-67].

The simulated SSTs closely match the observations in all simulations, indicating a high level of credibility in the simulations. In the VSCS Yaas case, the maximum error ranges between 3-4ºC for the 72-hour simulation (Table 4). However, for all other simulations, the errors remain at a lower level, ranging between 1-2ºC.

The recorded maximum low-level RV values for Fani, Yaas, Burevi, and DD cases are 100, 100-120, 100, and $100 \times 10^{-5}\ s^{-1}$ respectively [63, 65-67]. The simulated RV values are positive and correlate well with the observed data. The maximum error for low-level RV is $60 \times 10^{-5}\ s^{-1}$ in the 72-hour simulation, whereas the minimum error is $20 \times 10^{-5}\ s^{-1}$ in the 48-hour simulation. The RV generated by the 24-hour simulation in the DD case is approximately $50 \times 10^{-5}\ s^{-1}$. Notably, this is the only simulation where the simulated results are lower than the observations. However, the predicted RV findings are still reasonable and sufficient to maintain a strong cyclonic circulation.

The VWS values at both 850-200 hPa and 850-500 hPa levels are presented in Table 5, alongside the corresponding observed data. The observed VWS values for Fani, Yaas, Burevi, and DD cases are low to moderate and are recorded as 7-11, 5-11, 3-8, and 3-6 $m\,s^{-1}$ respectively. In comparison to the observations, the simulated VWS values between 850-200 hPa are significantly higher. However, the VWS values between 850-500 hPa vary from low to moderate, exhibiting commendable consistency with the actual data.

The simulated results appeared to be significantly higher than the observations during the 72-hour simulation. However, the predicted outcomes for the 24-hour lead time simulations are noticeably consistent with the observations [49, 53, 103-105]. Considering the error analysis, it can be concluded that if the lead time is reduced, the simulated results become very close to the observations. It is also determined that the model can reasonably generate the cyclonic systems but tends to generate higher intensities compared to the observations[49, 53, 103-107]. To leverage these outcomes, integrate diminished lead time simulations for TC formation and intensification forecasting system. This approach, combined with the RGPPI, can improve the accuracy and timeliness of forecasts, enhancing preparedness in vulnerable regions. This will assist sectors such as agriculture, transportation, and disaster management [108, 109]. Further research should focus on optimizing this integration into decision-making processes, enhancing their practical utility. Additionally, these findings can refine climate models and improve our understanding of short-term weather phenomena.

Table 3. Comparison of model simulated MCP and MSWS results with IMD's observation

Cases	Lead time (hour)	MCP (hPa)			MSWS ($m\,s^{-1}$)		
		Model	RSMC	Error	Model	RSMC	Error
Fani	72	965	997	32	65	15.42	49.48
	48	975		22	45		29.58
	24	990		07	35		19.58
Yaas	72	965	990	25	55	17.90	37.10
	48	975		15	45		27.10
	24	984		06	40		22.10
Burevi	72	975	1000	25	55	15.42	39.58
	48	981		19	45		29.58
	24	1000		00	27		11.58
DD	72	980	1002	22	50	15.42	34.58
	48	996		06	30		14.58
	24	1003		01	20		04.58

Table 4. Comparison of simulated SST and low-level RV results with IMD's observations

Cases	Lead time (hour)	SST (ºC)			Low-level RV (× 10^{-5} s^{-1})		
		Model	RSMC	Error	Model	RSMC	Error
Fani	72	27-30	30-31	1-3	160	100	60
	48	27-29		2-3	120		20
	24	27-29		2-3	140		40
Yaas	72	27	30-31	3-4	120	100-120	0-20
	48	29		1-2	150		30-50
	24	29		1-2	120		0-20
Burevi	72	28-30	29-30	1-2	140	100	40
	48	28-31		1-2	140		40
	24	28-32		1-2	170		70
DD	72	28-32	29-30	1-2	140	100	40
	48	28-32		1-2	120		20
	24	28-32		1-2	50		50

Table 5. Comparison of simulated maximum VWS results with IMD's observations

Cases	Lead time (hour)	Maximum VWS (m s^{-1})		
		VWS82	VWS85	RSMC
Fani	72	25-40	5-10	7-11
	48	20-30	5-10	
	24	20-30	5 -15	
Yaas	72	20-30	10-20	5-11
	48	25-30	10-15	
	24	25-30	15-25	
Burevi	72	25-30	5-20	3-8
	48	25-30	5-15	
	24	25-30	3-12	
DD	72	20-35	5-15	3-6
	48	25-30	5-10	
	24	25-30	3-9	

6. Conclusion

This study aims to develop a technique that will contribute to better comprehending the formation and intensification of TCs over the BoB. A strategy named RGPPI has been presented, and its potential for understanding cyclogenesis has been examined. The discussion of the aforementioned topic generates the following crucial conclusions:

- The proposed RGPPI technique is capable of generating realistic predictions regarding the genesis and development of cyclonic disturbances over the BoB compared to the GPPI.
- The average RGPPI values could be 3-8 times higher than the threshold value of 30 for severe systems.
- Mid-tropospheric instability, relative humidity at 850 hPa level, and vorticity at 850 hPa level are found to be key factors that influence the formation and intensification of TCs over the BoB.
- Upper-level VWS has negligible impact on the development of cyclonic systems, especially when there's low to moderate VWS up to the middle of the troposphere. This is especially true when there's strong instability in the middle of the troposphere, along with high humidity and vorticity at the 850 hPa level. This matches what we've found before [88, 89].
- Simulations with shorter lead times, especially those predicting 24 to 48 hours in advance, produced results that matched what was observed.

TC activity over the BoB is closely linked to the RGPPI technique. This approach provides insights into the potential severity and development of simulated systems within a 24 to 48-hour timeframe. It's noteworthy that realistic predictions have been made between 24 and 48 hours before the event, with no missed detections. However, in the DD case, the RGPPI predicted its development into a cyclonic storm during the 72-hour simulation, but this outcome wasn't realistic. Overestimation of the RGPPI value in the 72-hour simulation could occur due to the model's tendency to intensify systems in genesis simulations with longer lead time durations[47, 51, 88, 89]. Each parameter included in RGPPI plays a distinct role in the intensification of a low-pressure system. This metric would be crucial in determining the potential of a TC in its early stages. The insights from this technique would be valuable for operational forecasters. While the results from the case studies on cyclonic systems are promising, further studies can be conducted to establish threshold values and gain a more comprehensive understanding of RGPPI techniques.

Declaration of Competing Interest

The authors declare that they have no known competing financial interests or personal relationships that could have appeared to influence the work reported in this paper.

Limitations of the Study

In this study, the authors were unable to access the observed datasets comprising time series data for the studied parameters due to unavailability. Consequently, the simulated findings could not be validated in terms of

time series representation. Validation of simulated findings through time series representation in comparison to observations would be a valuable addition. The authors analyzed only four cases across the BoB. A larger number of cases from several basins can be studied to evaluate and improve the efficacy of this approach.

References

1) R.A.J. Pielke, J. Gratz, C.W. Landsea, D. Collins, A. Saunders, and R. Musulin, "Normalized hurricane damage in the United States: 1900-2005," *Nat. Hazards Rev.*, 9(1), 29–42 (2008). doi: 10.1061/(ASCE)1527-6988(2008)9:1(29)
2) P. Peduzzi, B. Chatenoux, H. Dao, A.D. Bono, C. Herold, J. Kossin, F. Mouton, and O. Nordbeck, "Global trends in tropical cyclone risk," *Nature Climate Change,* 2(4), 289–294 (2012). doi: 10.1038/nclimate1410
3) W.M. Gray, "Hurricanes: Their formation, structure and likely role in the tropical circulation. Meteorology over the Tropical Oceans," D. B. Shaw, Ed., Royal Meteorological Society, 155–218 (1979).
4) C.J. Neumann, "Global overview. In: Global guide to tropical cyclone forecasting," World Meteorological Organization, Geneva, 1.1–1.56 (1993). Available at: https://cyclone.wmo.int/
5) M.M. Alam, M.A. Hossain, and S. Shafee, "Frequency of Bay of Bengal cyclonic storms and depressions crossing different coastal zones," *Int. J. Climatol.,* 23, 1119–1125 (2003). doi:10.1002/joc.927
6) RSMC, "Tracks of cyclones and depressions over the North Indian Ocean (from 1891 onwards) (Cyclone eAtlas - IMD, Version 2.0)," Cyclone Warning and Research Centre, India Meteorological Department, Regional Meteorological Centre, Chennai, 2011.
7) P.S. Chittibabu, K. Dube, J.B. Macnabb, T.S. Murty, A. D. Rao, U.C. Mohanty, and P.C. Sinha, "Mitigation of flooding and cyclone hazard in Orissa, India," *Nat. Hazards,* 31(2), 455–485 (2004). doi: 10.1023/B:NHAZ.0000023362.26409.22
8) H.M. Fritz, C.D. Blount, S. Thwin, M.K. Thu, N. Chan, "Cyclone Nargis storm surge in Myanmar," *Nat. Geosci.*, 2, 448-449 (2009). doi:10.1038/ngeo558
9) M. Ozaki, "Disaster Risk Financing in Bangladesh," *ADB South Asia working paper series,* 46, 1-35 (2016). Available at: https://www.adb.org/sites/default/files/publication/198561/sawp-046.pdf
10) K. Emanuel, "Increasing destructiveness of tropical cyclones over the past 30 years," *Nature,* 436, 686–688 (2005). https://doi.org/10.1038/nature03906
11) I. Hossain, and A.R. Mullick, "Cyclone and Bangladesh: A Historical and Environmental Overview from 1582 to 2020," *International Medical Journal*, 25(6), 2595–2614 (2020).
12) M.A. Bender, T.R. Knutson, R.E. Tuleya, J.J. Sirutis, G.A. Vecchi, S.T. Garner, and I.M. Held, "Modeled impact of anthropogenic warming on the frequency of intense Atlantic hurricanes," *Science*, 327, 454–458 (2010). doi:10.1126/science.1180568
13) L. Bengtsson, K.I. Hodges, M. Esch, N. Keenlyside, L. Kornblueh, J.J. Luo, and T.T. Yamagata, "How may tropical cyclones change in a warmer climate?," *Tellus A: Dynamic Meteorology and Oceanography*, 59(4), 539-561 (2007). doi:10.1111/j.1600-0870.2007.00251.x
14) M. Zhao, I.M. Held, S.J. Lin, and G.A. Vecchi, "Simulations of global hurricane climatology, interannual variability, and response to global warming using a 50-km resolution GCM," *J. Climate,* 22(24), 6653–6678 (2009). doi:10.1175/2009JCLI3049.1
15) T.R. Knutson, J.J. Sirutis, S.T. Garner, I.M. Held, and R.E. Tuleya, "Simulation of the recent multidecadal increase of Atlantic hurricane activity using an 18-km-grid regional model," *Bull. Amer. Meteor. Soc.,* 88(10), 1549–1565 (2007). doi:10.1175/BAMS-88-10-1549
16) W.M. Gray, "Global view of the origin of tropical disturbances and storms," *Mon. Wea. Rev.,* 96(10), 669–700 (1968). doi:10.1175/1520-0493(1968)096%3C0669:GVOTOO%3E2.0.CO;2
17) H. Riehl, "On the formation of typhoons," *Journal of the Atmospheric Sciences,* 5(6), 247–265 (1948). doi:10.1175/1520-0469(1948)005%3C0247:OTFOT%3E2.0.CO;2
18) R. Rotunno, and K.A. Emanuel, "An air-sea interaction theory for tropical cyclones. Part II. Evolutionary study using a nonhydrostatic axisymmetrical numerical model," *J. Atmos. Sci.,* 44(3), 542–561 (1987). doi:10.1175/1520-0469(1987)044%3C0542:AAITFT%3E2.0.CO;2
19) K. Emanuel, "Tropical cyclones," *Annual Review of Earth and Planetary Sciences,* 31, 75–104 (2003). doi: 10.1146/annurev.earth.31.100901.141259
20) K.A. Emanuel, and D.S. Nolan, "Tropical cyclone activity and global climate," Proc. of 26th Conference on Hurricanes and Tropical Meteorology, American Meteorological Society, Miami, FL, 2004.
21) J. Ren, J.A. Zhang, J.L. Vigh, P. Zhu, H. Liu, X. Wang, and J.B. Wadler, "An Observational Study of the Symmetric Boundary Layer Structure and Tropical Cyclone Intensity," *Atmosphere,* 11(2), 158, (2020). doi:10.3390/atmos11020158
22) D.S. Gutzler, K.M. Wood, E.A. Ritchie, A.V. Douglas, and M.D. Lewis, "Interannual variability of tropical cyclone activity along the Pacific coast of North America," *Atmosfera,* 26(2), 149–162 (2013). doi:10.1016/S0187-6236(13)71069-5
23) D. Raymond, S. Sessions, and C.L. Carrillo, "Thermodynamics of tropical cyclogenesis in the

northwest Pacific," *J. Geophys. Res. Atmos*., 116, 2011. doi:10.1029/2011JD015624

24) J.L. McBride, and R. Zeh, "Observational analysis of tropical cyclone formation. Part II: Comparison of non-developing versus developing systems," *J. Atmos. Sci.,* 38(6), 1132–1151 (1981). doi:10.1175/1520-0469(1981)038%3C1132:OAOTCF%3E2.0.CO;2
25) J. Simpson, E. Ritchie, G.J. Holland, J. Halverson, and S. Stewart, "Mesoscale interactions in tropical cyclone genesis," *Mon. Wea. Rev.,* 125(10), 2643–2661 (1997). doi:10.1175/1520-0493(1997)125%3C2643:MIITCG%3E2.0.CO;2
26) T.J. Dunkerton, M.T. Montgomery, and Z. Wang, "Tropical cyclogenesis in a tropical wave critical layer: Easterly waves," *Atmos. Chem. Phys*., 9(15), 5587–5646 (2009). doi:10.5194/acpd-8-11149-2008
27) G. Kutty, and K. Gohil, "The role of mid-level vortex in the intensification and weakening of tropical cyclones," *J. Earth Syst. Sci.,* 126(7), 2017. doi:10.1007/s12040-017-0879-y
28) A.M. Makarieva, V.G. Gorshkov, A.V. Nefiodov, A.V. Chikunov, D. Sheil, A.D. Nobre, and B.L. Li, "Fuel for cyclones: The water vapor budget of a hurricane as dependent on its movement," *Atmos. Res*., 193, 216–230 (2017). doi:10.1016/j.atmosres.2017.04.006
29) K. Fujiwara, R. Kawamura, H. Hirata, T. Kawano, M. Kato, and T. Shinoda, "A positive feedback process between tropical cyclone intensity and the moisture conveyor belt assessed with Lagrangian diagnostics," *J. Geophys. Res. Atmos.*, 122(23), 12502–12521 (2017). doi:10.1002/2017JD027557
30) R. Yoshida, Y. Miyamoto, H. Tomita, Y. Kajikawa, "The effect of water vapor on tropical cyclone genesis: A numerical experiment of a non-developing disturbance observed in PALAU2010," *J. Meteor. Soc. Japan,* 95(1), 35–47 (2017). doi:10.2151/jmsj.2017-001
31) M. DeMaria, "The effect of vertical shear on tropical cyclone intensity change," *Journal of the Atmospheric Sciences*, 53(14), 2076–2087 (1996). doi:10.1175/1520-0469(1996)053%3C2076:TEOVSO%3E2.0.CO;2
32) W.M. Frank, and E.A. Ritchie, "Effects of vertical wind shear on the intensity and structure of numerically simulated hurricanes," *Mon. Wea. Rev*., 129(9), 2249–2269 (2001). doi:10.1175/1520-0493(2001)129%3C2249:EOVWSO%3E2.0.CO;2
33) S.A. Khan, A. Ranjan, K. Harish, and P.K. Arora, "A Perspective on Advances in Cloud-based Additive Manufacturing," *Evergreen*, 9(3), 861-869 (2022). doi:10.5109/4843119
34) M. Al-Ghriybah, "Assessment of Wind Energy Potentiality at Ajloun, Jordan Using Weibull Distribution Function," *Evergreen*, 9(1), 10-16, (2022). doi:10.5109/4774211
35) T.C. Rudien, D.H. Didane, M.F.M. Batch, K. Abdullah, S. Mohd, B. Manshoor, and S. Al-Alimi, "Technical Feasibility Analysis of Wind Energy Potentials in two sites of East Malaysia: Santubong and Kudat," *Evergreen*, 8(2), 271-279, (2021). doi:10.5109/4480703
36) N. Hasbullah, F.A.Z. M. Saat, F. S. Anuar, D. Johari, and M.F. Sukri, "Temperature and Velocity Changes Across Tube Banks in One- directional and Bi-directional Flow Conditions," *Evergreen*, 8(2), 428-437, (2021). doi:10.5109/4480725
37) A.S. Baskoro, M.A. Amat, R.D. Putra, A. Widyianto, and Y. Abrara, "Investigation of Temperature History, Porosity and Fracture Mode on AA1100 Using the Controlled Intermittent Wire Feeder Method," *Evergreen*, 7(1), 86-91, (2020). doi:10.5109/2740953
38) S.K. Gupta, and V.K. Dwivedi, "Prediction of Depth Ratio, Jump Length and Energy Loss in Sloped Channel Hydraulic Jump for Environmental Sustainability," *Evergreen*, 10(2), 942-952, (2023). doi:10.5109/6792889
39) A. Sharma, H. Chawla, and K. Srinivas, "Prediction of Surface Roughness of Mild Steel finished with Viscoelastic Magnetic Abrasive Medium," *Evergreen*, 10(2), 1061-1067, (2023). doi:10.5109/6793663
40) D.P. Sari, A. Sumarno, A.M. Prasetyo, Maidina, and L.N. Ngeljaratan, "Energy Conservation Techniques in Tropical Climate - A Comprehensive Review and Adaptation of the Lamin House for Nusantara," *Evergreen*, 10(3), 2021-2028, (2023). doi:10.5109/7151769
41) H. Halidah, N. Hesty, P. Aji, Ifanda, D. Amelia, and K. Akhmad, "Short-Term Wind Forecasting with Weather Data using Deep Learning - Case Study in Baron Techno Park," *Evergreen*, 10(3), 1753-1761, (2023). doi:10.5109/7151724
42) B. Utomo, H. Firdaus, Q. Lailiyah, N. Kusnandar, I. Supono, I. Paramudita, and W.P. Syam, "Investigation the Effect of Various Temperature-Measuring Configurations on The Thermal Efficiency of Liquid Petroleum Gas Stoves," *Evergreen*, 10(3), 1651-1659, (2023). doi:10.5109/7151713
43) B.B. Alikhanov, S.V. Samoilov, V.I. Sokolov, and L.P. Seitova, "Theory of Climate Change Intensity Determination," *Evergreen*, 10(3), 1253-1260, (2023). doi:10.5109/7148446
44) A. Aitimbetova, A. Batyrkhanova, A. Nurtayeva, R. Isayeva, and G. Bektureyeva, "Environmental Assessment of Solid Waste Pollution of Urban Areas (on the example of Shymkent, Republic of Kazakhstan)," *Evergreen*, 10(3), 1209-1217, (2023). doi:10.5109/7148441
45) A. Yussupov, and R.Z. Suleimenova, "Use of Remote Sensing Data for Environmental Monitoring of

Desertification," *Evergreen*, 10(1), 300-307, (2023). doi:10.5109/6781080

46) P.J. Sousounis, T.A. Hutchinson, and S.F. Marshall, "A comparison of MM5, WRF, RUC, and ETA performance for great plains heavy precipitation events during the spring of 2003," Preprints 20th Conference on Weather Analysis and Forecasting, Seattle, Amer. Meteo. Soci., 2004.
47) W.Y.Y. Cheng, and W.J. Steenbyrgh, "Evaluation of surface sensible weather forecasts by WRF and ETA models over the Western United States," *Weather Forecast.,* 20, 812–821 (2005). doi:10.1175/WAF885.1
48) P. Sujatha, and U.C. Mohanty, "A Comparative study on prediction of MM5 and WRF models in simulation of tropical cyclones over Indian seas," *Curr. Sci.,* 95(7), 923–936 (2008). https://www.jstor.org/stable/24103192
49) M.S. Hossain, M.A. Samad, S.M.A. Hossen, S.M.Q. Hassan, and M.A.K. Malliak, "The Efficacy of the WRF-ARW Model in the Genesis and Intensity Forecast of Tropical Cyclone Fani over the Bay of Bengal," *Journal of Engineering Science,* 12(3), 85-100 (2021). doi:10.3329/jes.v12i3.57482
50) R. Rogers, S. Aberson, and Coauthors, "NOAA'S Hurricane Intensity Forecasting Experiment: A Progress Report," *Bulletin of the American Meteorological Society,* 94(6), 859-882 (2013). doi:10.1175/bams-d-12-00089.1
51) S. Kanada, and A. Wada, "Sensitivity to Horizontal Resolution of the Simulated Intensifying Rate and Inner-Core Structure of Typhoon Ida, an Extremely Intense Typhoon," *Journal of the Meteorological Society of Japan Ser II*, 94, 181-190 (2016). doi:10.2151/jmsj.2015-037
52) W.M. Chen, M.T. Kueh, Y.F. Sheng, and C.L. Simon, "Effects of horizontal resolution and air-sea flux parameterization on the intensity and structure of simulated Typhoon Haiyan (2013)," *Natural Hazards and Earth System Sciences*, 19(7), 1509-1539 (2013). doi:10.5194/nhess-19-1509-2019
53) M.S. Hossain, M.A. Samad, M.S. Hossain, S.M.A. Hossen, M.A. Islam, and S.M.A. Hassan, "The Sensitivity of Initial Condition and Horizontal Resolution on Simulation of Tropical Cyclone Amphan over the Bay of Bengal using WRF-ARW Model," *Dhaka Univ. J. Sci*., 69(3), 202-211 (2022). doi:10.3329/dujs.v69i3.60031
54) C.V. Srinivas, D.V. Bhaskar Rao, V. Yesubabu, R. Baskaran, and B. Venkatraman, "Tropical cyclone predictions over the Bay of Bengal using the high-resolution advanced research weather research and forecasting model," *Q. J. R. Meteorol. Soc.,* 139, 1810 – 1825 (2012). doi:10.1002/qj.2064
55) S.K. Roy Bhowmik, "An evaluation of cyclone genesis parameter over the Bay of Bengal using model analysis," *Mausum*, 54(2), 351-358 (2003). doi:10.54302/mausam.v54i2.1520
56) C. Gao, L. Zhou, C. Wang, I.I. Lin, and R. Murtugudde, "Unexpected limitation of tropical cyclone genesis by subsurface tropical central-north Pacific during El Niño," *Nat. Commun.,* 13, (2022). doi:10.1038/s41467-022-35530-9
57) K. Emanuel, "The dependence of hurricane intensity on climate," *Nature*, 326, 483–485 (1987). doi:10.1111/j.1600-0870.2007.00238.x
58) S.J. Camargo, K.A. Emanuel, and A.H. Sobal, "Use of a genesis potential index to diagnose ENSO effects on tropical cyclone genesis," *J. Clim*., 20(19*)*, 4819–4834 (2007b). doi:10.1175/JCLI4282.1
59) S.J. Camargo, A.H. Sobel, A.G. Barnston, and K.A. Emanuel, "Tropical cyclone genesis potential index in climate models," *Tellus A: Dynamic Meteorology and Oceanography*, 59(4), 428–443 (2007a). doi:10.1111/j.1600-0870.2007.00238.x
60) H. Murakami, and B. Wang, "Future change of north Atlantic tropical cyclone tracks, Projection by a 20 km mesh global atmospheric model," *J. Clim.,* 23(10), 2699–2721 (2010). doi:10.1175/2010JCLI3338.1
61) I.F. Pun, I.I. Lin, and M.H. Lo, "Recent increase in high tropical cyclone heat potential area in the Western North Pacific Ocean," *Geophys. Res. Lett*., 40(17), 4680–4684 (2013). doi:10.1002/grl.50548
62) S.D. Kotal, P.K. Kundu, and S.K. Roy Bhowmik, "Analysis of cyclogenesis parameter for developing and nondeveloping low-pressure systems over the Indian Sea," *Nat. Hazards,* 50, 389–402 (2009). doi:10.1007%2Fs11069-009-9348-5
63) P. Suneeta and S.S.V.S. Ramakrishna, "Modified tropical cyclone genesis potential index over the Bay of Bengal during southwest and post-monsoon seasons," *J. Earth Syst. Sci.,* 130, (2021). doi:10.1007/s12040-021-01700-4
64) M. DeMaria, J.A. Knaff, and B.H. Connell, "A Tropical Cyclone Genesis Parameter for the Tropical Atlantic," *Wea. Forecasting*, 16(2), 219–233 (2001). doi:10.1175/1520-0434(2001)016%3C0219:ATCGPF%3E2.0.CO;2
65) A. Routray, A. Lodh, D. Dutta, J.P. George, "Study of an Extremely Severe Cyclonic Storm "Fani" over the Bay of Bengal using regional NCUM modeling system: A case study," *Journal of Hydrology*, 590, 2020. doi: 10.1016/j.jhydrol.2020.125357
66) V. Singh, R.T. Konduru, A.K. Srivastava, I.M. Momin, S. Kumar, A.K. Singh, D.S. Bisht, S. Tiwari, A.K. Sinha, "Predicting the rapid intensification and dynamics of pre-monsoon extremely severe cyclonic storm 'Fani' (2019) over the Bay of Bengal in a 12-km global model," *Atmospheric Research*, 247, 2020. doi: 10.1016/j.atmosres.2020.105222
67) M.S. Hossain, M.A. Samad, M.R. Sultana, M.A.K. Mallik, and M.J. Uddin, "Track and Landfall Characteristics of Very Severe Cyclonic Storm Fani

over the Bay of Bengal using WRF Model," Dhaka Univ. J. Sci., 69(2), 101-108 (2021). doi:10.3329/dujs.v69i2.56490

68) RSMC, "*Extremely Severe Cyclonic Storm "FANI" over eastcentral equatorial Indian Ocean and adjoining southeast Bay of Bengal (26 April – 04 May, 2019): Summary; Regional specialised meteorological centre tropical cyclones*," Cyclone Warning Division, India Meteorological Department, New Delhi, (2019). Available at: https://rsmcnewdelhi.imd.gov.in/uploads/report/26/26_7122ae_Preliminary%20Report%20on%20ESCS%20FANI_15082020.pdf
69) P. Bhardwaj, and O. Singh, "*Understanding the Development and Progress of Extremely Severe Cyclonic Storm "Fani" Over the Bay of Bengal*," In: Shit, P.K., Pourghasemi, H.R., Bhunia, G.S., Das, P., Narsimha, A. (eds) Geospatial Technology for Environmental Hazards. Advances in Geographic Information Science. Springer, (2022). doi:10.1007/978-3-030-75197-5_12
70) S. Paul, and S. Chowdhury, "Investigation of the character and impact of tropical cyclone Yaas: a study over coastal districts of West Bengal, India," Safety in Extreme Environments, 3, 219–235 (2021). doi: 10.1007/s42797-021-00044-y
71) S. Chatterjee, and B. Biswas, "Cyclone Yaas: A Curse to Coastal People of Odisha and West Bengal (India)," *Natl. Acad. Sci. Lett*., 46(4), 321–324 (2023). doi: 10.1007/s40009-023-01251-w
72) RSMC, "*Very Severe Cyclonic Storm YAAS over the Bay of Bengal (23rd – 28th May, 2021): A Report*," Cyclone Warning Division, India Meteorological Department, New Delhi, (2021). Available at: https://rsmcnewdelhi.imd.gov.in/uploads/report/26/26_77afd4_Preliminary%20Report%20YAAS%20during%2023-27%20May%202021.pdf
73) G.K. Das, Climatic Hazards of the Coast. In: Coastal Environments of India. Springer Water. Springer, Cham. doi:10.1007/978-3-031-18846-6_8
74) A. Sarkar, S. Kumar, A. Dube, S.K. Prasad, A. Mamgain, P. Chakraborty, R. Ashrit. and A.K. Mitra, "Forecasting of tropical cyclone using global and regional ensemble prediction systems of NCMRWF: A review," Mausam, 72(1), 77-86 (2021). doi: 10.54302/mausam.v72i1.131
75) G.K. Das, "cyclonic hazards in the recent past in Peninsular India," Reason-A Technical Journal, 1-15 (2020). doi: 10.21843/reas/2020/1-15/209270.
76) RSMC, "*Cyclonic Storm, 'BUREVI' over the Bay of Bengal (30th November - 05th December 2020): A Report*," Cyclone Warning Division, India Meteorological Department, New Delhi, (2019). Available at: https://rsmcnewdelhi.imd.gov.in/uploads/report/26/26_0522b4_burevi.pdf
77) RSMC, "*Deep Depression over Southeast Bay of Bengal (06-09 December, 2017): A Report*," Cyclone Warning Division, India Meteorological Department, New Delhi, (2017). Available at: https://rsmcnewdelhi.imd.gov.in/uploads/report/26/26_dad038_dd06-09dec.pdf
78) J.S. Kain, "The Kain–Fritsch Convective Parameterization, An Update," *J. Appl. Meteor*., 43(1), 170-181 (2004). doi:10.1175/1520-0450(2004)043%3C0170:TKCPAU%3E2.0.CO;2
79) E. Kessler, "On the distribution and continuity of water substance in atmospheric circulations," *Meteor. Monogr.*, 32, 1-48 (1969). doi:10.1007/978-1-935704-36-2_1
80) S.Y. Hong, "A new vertical diffusion package with an explicit treatment of entrainment processes," *Mon. Wea. Rev.*, 134(9), 2318–2341 (2006). doi:10.1175/MWR3199.1
81) P.A. Jimenez, J. Dudhia, F.G. Rouco, J. Navarro, J.P. Montavez, and E.G. Bustamante, "A revised scheme for the WRF surface layer formulation," *Mon. Wea. Rev*., 140(3), 898–918 (2012). doi:10.1175/MWR-D-11-00056.1
82) M. Tewari, F. Chen, W. Wang, J. Dudhia, M.A. LeMone, K. Mitchell, M. Ek, G. Gayno, J. Wegiel, and R.H. Cuenca "Implementation and verification of the unified NOAH land surface model in the WRF model," 20th Conference on Weather Analysis and Forecasting/16th Conference on Numerical Weather Prediction, (2004).
83) J. Dudhia, "Numerical study of convection observed during the Winter Monsoon Experiment using a mesoscale two–dimensional model," *J. Atmos. Sci*., 46(20), 3077–3107 (1989). doi:10.1175/1520-0469(1989)046%3C3077:NSOCOD%3E2.0.CO;2
84) E.J. Mlawer, S.J. Taubman, P.D. Brown, M.J. Iacono, and S.A. Clough, "Radiative transfer for inhomogeneous atmospheres: RRTM, a validated correlated–k model for the longwave," *J. Geophys. Res.,* 102, 16663–16682 (1997). doi:10.1029/97JD0023
85) T. Miyasaka, and H. Nakamura, "Structure and Formation Mechanisms of The Northern Hemisphere Summertime Subtropical Highs," *Journal of Climate,* 18(23), 5046-5065 (2005). doi:10.1175/JCLI3599.1
86) U. Loptien, O. Zolina, S. Gulev, M. Latif, and V. Soloviov, "Cyclone life cycle characteristics over the Northern Hemisphere in coupled GCMs," *Climate Dynamics,* 31(5), 507-532 (2008). doi:10.1007/s00382-007-0355-5
87) E.P. Lim, and I. Simmonds, "Explosive Cyclone Development in the Southern Hemisphere and a Comparison with Northern Hemisphere Events," *Monthly Weather Review,* 130(9), 2188–2209 (2002). doi:10.1175/1520-0493(2002)130%3C2188:ECDITS%3E2.0.CO;2

88) V.K. Singh, M.K. Roxy, and M.M. Deshpande, "Role of warm ocean conditions and the MJO in the genesis and intensification of extremely severe cyclone Fani," *Scientific Reports,* 11, (2021). doi:10.1038/s41598-021-82680-9

89) A.R. Aiyyer and C. Thorncroft, "Climatology of Vertical Wind Shear over the Tropical Atlantic," *Journal of Climate,* 19(12), 2969–2983 (2006). doi:10.1175/JCLI3685.1

90) K.L. Corbosiero, and J. Molinari, "The Relationship between Storm Motion, Vertical Wind Shear, and Convective Asymmetries in Tropical Cyclones," *Journal of the Atmospheric Sciences*, 60(2), 366–376 (2003). doi:10.1175/1520-0469(2003)060%3C0366:TRBSMV%3E2.0.CO;2

91) N. Sharma, and A.K. Varma, "Impact of vertical wind shear in modulating tropical cyclones eye and rainfall structure," *Natural Hazards*, 112, 2083–2100 (2022). doi:10.1007/s11069-022-05257-3

92) D.S. Nolan, E.D. Rappin, and K.A. Emanuel, "Tropical cyclogenesis sensitivity to environmental parameters in radiative-convective equilibrium," *Quart. J. Roy. Meteor. Soc*., 133, 2085–2107 (2007). doi:10.1002/qj.170

93) M.S. Peng, B. Fu, T. Li, and D.E. Stevens, "Developing versus Non developing Disturbances for Tropical Cyclone Formation. Part I: North Atlantic," *Monthly Weather Review*, 140(4), 1047–1066 (2012a). doi:10.1175/2011MWR3617.1

94) M.S. Peng, B. Fu, T. Li, and D.E. Stevens, "Developing versus Non developing Disturbances for Tropical Cyclone Formation. Part II: Western North Pacific," *Monthly Weather Review,* 140(4), 1067–1080 (2012b). doi:10.1175/2011MWR3618.1

95) W. Li, C. Wang, D. Wang, and L. Yang, "Modulation of Low-Latitude West Wind on Abnormal Track and Intensity of Tropical Cyclone Nargis (2008) in the Bay of Bengal," *Advances in Atmospheric Sciences,* 29(2), 407–421 (2012). doi:10.1007/s00376-011-0229-y

96) T. Schott et al., "The Saffir-Simpson hurricane wind scale," National Weather Services, National Hurricane Centre, National Oceanic and Atmospheric Administration (NOAA) factsheet, (2012). Retrieved from http://www.nhc.noaa.gov/pdf/sshws.pdf

97) D.R. Chavas, K.A. Reed, and J.A. Knaff, "Physical understanding of the tropical cyclone wind-pressure relationship," *Nature Communications*, 8, (2017). doi:10.1038/s41467-017-01546-9

98) B.K. Mahala, P.K. Mohanty, M. Das, and A. Routray, "Performance assessment of WRF model in simulating the very severe cyclonic storm "TITLI" in the Bay of Bengal: A case study," *Dynamics of Atmospheres and Oceans,* 88, (2019). doi:10.1016/j.dynatmoce.2019.101106

99) M. Mandal, K.S. Singh, M. Balaji, and M. Mohapatra, "Performance of WRF-ARW model in real-time prediction of Bay of Bengal cyclone Phailin," *Pure and Applied Geophysics,* 173, 1783–1801 (2016). doi:10.1007/s00024-015-1206-7

100) J.P. Terry, "Tropical Cyclones: Climatology and Impacts in the South Pacific," Springer New York, NY, (2010). doi:10.1007/978-0-387-71543-8

101) S. Kotal, and S.A. Bhattacharya, "Tropical cyclone Genesis Potential Parameter (GPP) and its application over the north Indian Sea," *Mausum*, 64(1), 149–170 (2013). doi:10.54302/mausam.v64i1.663

102) Z. Li, W. Yu, K. Li, H. Wang H, and Y. Liu, "Environmental Conditions Modulating Tropical Cyclone Formation over the Bay of Bengal during the Pre-Monsoon Transition Period," *Journal of Climate*, 32(14), 4387–4394 (2019). doi:10.1175/JCLI-D-18-0620.1

103) K.K. Osuri, K. Ankur, R. Nadimpalli, and N.K.R. Busireddy, "Error characterization of ARW model in Forecasting tropical cyclone rainfall over North Indian Ocean," *Journal of Hydrology*, 590, 2020. doi: 10.1016/j.jhydrol.2020.125433

104) C.V. Srinivas, D.V. Bhaskar Rao, V. Yesubabu, R. Baskaran, B. Venkatraman, "Tropical cyclone predictions over the Bay of Bengal using the high-resolution Advanced Research Weather Research and Forecasting (ARW) model," *Q. J. R. Meteorol. Soc.*, 139(676), 1810-1825 (2013). doi: 10.1002/qj.2064

105) K.K. Osuri, U.C. Mohanty, A. Routray, M.A. Kulkarni, and M. Mohapatra, "Customization of WRF-ARW model with physical parameterization schemes for the simulation of tropical cyclones over North Indian Ocean," *Nat. Hazards.*, 63, 1337–1359 (2012). doi:10.1007/s11069-011-9862-0

106) K.S. Singh, J. Albert, P.K. Bhaskaran, and P. Alam, "Assessment of extremely severe cyclonic storms over Bay of Bengal and performance evaluation of ARW model in the prediction of track and intensity," *Theor. Appl. Climatol*., 143, 1181–1194 (2021). doi:10.1007/s00704-020-03510-y

107) P. Mukherjee and B. Ramakrishnan, "On the understanding of very severe cyclone storm Ockhi with the WRF-ARW model," *Environmental Research: Climate*, 1(1), (2022). doi: 10.1088/2752-5295/ac6adb

108) B. Sahoo, P.K. Bhaskaran, and A.K. Pradhan, "Application of weather forecasting model WRF for operational electric power network management—a case study for Phailin cyclone," *Theor. Appl. Climatol*., 137, 871–891 (2019). doi:10.1007/s00704-018-2639-6

109) L. Xue, Y. Li, L. Song, W. Chen, and B. Wang, "A WRF-based engineering wind field model for tropical cyclones and its applications," *Nat. Hazards*, 87, 1735–1750 (2017). doi:10.1007/s11069-017-2845-z